Instructive role of MLL-fusion proteins revealed by a model of t(4;11) pro-B acute lymphoblastic leukemia

Lin, Shan; Luo, Roger T. ; Ptasinska, Anetta; Kerry, Jon; Assi, Salam; Wunderlich, Mark ; Lmamura, Toshihiko ; Kaberlein, Joseph J. ; Rayes, Ahmad ; Althoff, Mark J. ; Anastasi, John ; O'Brien, Maureen M. ; Meetei, Amom Ruhikanta; Milne, Thomas A.; Bonifer, Constanze; Mulloy, James; Thirman, Michael J.

DOI:
10.1016/j.ccell.2016.10.008

Document Version
Peer reviewed version

Citation for published version (Harvard):
Lin, S, Luo, RT, Ptasinska, A, Kerry, J, Assi, S, Wunderlich, M, Lmamura, T, Kaberlein, JJ, Rayes, A, Althoff, MJ, Anastasi, J, O'Brien, MM, Meetei, AR, Milne, TA, Bonifer, C, Mulloy, J & Thirman, MJ 2016, 'Instructive role of MLL-fusion proteins revealed by a model of t(4;11) pro-B acute lymphoblastic leukemia', *Cancer Cell*, vol. 30, no. 5, pp. 737–749. https://doi.org/10.1016/j.ccell.2016.10.008

Title: Instructive role of MLL-fusion proteins revealed by a faithful model of t(4;11) proB acute lymphoblastic leukemia

Authors:

Shan Lin[1†], Roger T. Luo[2†], Anetta Ptasinska[3], Jon Kerry[4], Salam A. Assi[3], Mark Wunderlich[1], Toshihiko Imamura[2], Joseph J. Kaberlein[2], Ahmad Rayes[1], Mark J Althoff[l], John Anastasi[5], Maureen M. O'Brien[1], Amom Ruhikanta Meetei[1], Thomas A. Milne[4], Constanze Bonifer[3], James C. Mulloy[1*] and Michael J. Thirman[2*]

Affiliations:

[1]Cancer and Blood Disease Institute, Cincinnati Children's Hospital Medical Center, Cincinnati, OH 45229.

[2]Department of Medicine, Section of Hematology/Oncology, University of Chicago, Chicago, IL, USA.

[3]School of Cancer Sciences, University of Birmingham, Birmingham, UK.

[4] MRC Molecular Haematology Unit, Weatherall Institute of Molecular Medicine, NIHR Oxford Biomedical Research Centre Programme,University of Oxford, Oxford OX3 9DS, UK.

[5]Department of Pathology, University of Chicago, Chicago, IL, USA.

[*]Correspondence to: james.mulloy@cchmc.org and mthirman@medicine.bsd.uchicago.edu

[†]These authors contributed equally to this work

Highlights

1. Fusion of MLL to murine Af4 permits faithful modeling of human t(4;11) proB ALL
2. The species of the cell-of-origin determines the lineage of MLL-Af4 leukemia
3. MLL-fusion proteins drive differential gene expression via specific genomic targets
4. MLL-fusion leukemia circumvents CD19-directed therapies through lineage plasticity

Summary

The t(4;11)(q21;q23) fuses MLL to AF4, the most common MLL-fusion partner. Here we show that MLL fused to murine Af4, highly conserved with human AF4, produces high-titer retrovirus permitting efficient transduction of human CD34+ cells and generating a faithful model of t(4;11) proB ALL that fully recapitulates the immunophenotypic and molecular aspects of the disease. MLL-Af4 induces a B-ALL distinct from MLL-AF9 through differential genomic target binding of the fusion proteins leading to specific gene expression patterns. MLL-Af4 cells can assume a myeloid state under environmental pressure but retain lymphoid-lineage potential. Such incongruity was also observed in t(4;11) patients who evaded CD19-directed therapy by undergoing myeloid-lineage switch. Our model provides a valuable tool to unravel the pathogenesis of MLL-AF4 leukemogenesis.

Significance

MLL-AF4 is associated with B-ALL and confers poor prognosis. The lack of an accurate model has hampered the study of disease pathobiology and therapeutic testing. We overcame previous limitations to retroviral production by fusing MLL to murine Af4. Transduced human CD34+

cells develop into a proB ALL faithful to t(4;11) disease, whereas MLL-Af4-transduced murine cells develop only AML, demonstrating the species-specificity of the fusion and highlighting the complexity of human disease modeling. We find that MLL-fusion leukemia shows genetic heterogeneity driven by differential genomic target binding of the different fusion proteins. We report lineage plasticity as a new mechanism of resistance to CD19-directed therapy in t(4;11) patients thus highlighting the clinic relevance of our model. This model can provide unique insight for targeting t(4;11) ALL.

Introduction

MLL-AF4 accounts for 10% of ALL associating with a unique proB immunophenotype and poor prognosis(Marchesi et al., 2011). A better understanding of disease pathogenesis and new therapeutic approaches are therefore needed to improve outcome. Much progress has been made in understanding MLL-rearranged leukemia and potential therapeutic targets were identified using mouse models. However, these models predominantly develop AML but not ALL(Krivtsov et al., 2008; Lavau et al., 1997). The chromatin binding capacity of MLL is retained in the fusion protein, with the fusion partner protein recruiting the super elongation complex (SEC) and other epigenetic regulators and leading to aberrant activation of MLL targets, including *HOXA* genes(Faber et al., 2009). It was assumed that these models would also shed light on MLL-fusion ALL, given that a common gene signature was identified among different MLL-fusion leukemia samples(Armstrong et al., 2002). However, differential sensitivities to target gene and pathway ablation are observed among MLL-fusion leukemia cells arguing that the knowledge generated from AML models may not be applicable to ALL(Liu et al., 2014). Moreover, although ALL with MLL-rearrangement has been generally considered as a

single pathologic entity, substantial fusion partner-specific transcription and epigenetic programs have been identified(Stam et al., 2010; Stumpel et al., 2011), although the underlying mechanism and biological consequence of this molecular heterogeneity is unclear. Thus, a faithful MLL-AF4 model is required to examine the mechanisms that mediate the unique features of the disease.

Until now, it was not possible to produce MLL-AF4 retrovirus with a high enough titer to efficiently transduce hematopoietic stem and progenitor cells (HSPC) from mice and humans. However, use of a hybrid *MLL-Af4* gene overcame these problems and we successfully established a faithful model mimicking the distinct immunophenotypic and molecular features of the disease. The necessity to express MLL-Af4 in human but not mouse HSPC to recapitulate the lymphoid features of t(4;11) leukemia highlights the complexity of accurately modeling human disease and has important implications for the development of mouse models of human disease. Our MLL-Af4 model will serve as a useful platform for the development of customized therapeutic targeting.

Results

MLL-Af4 produces high titer retrovirus permitting transformation of murine HSPC

We initially sought to establish a MLL-AF4 leukemia model in the mouse using a retroviral transduction approach. However, MLL-AF4 retroviral titers were consistently low, as reported by others(Bursen et al., 2010; Yokoyama et al., 2010), and thus inadequate for efficient transduction of murine HSPC(Kalberer et al., 2002). Multiple factors can affect viral titer production, and some human cDNAs have been found to dramatically decrease viral titers(Skalamera et al., 2012). Murine homologs of MLL and its partners have been employed in mouse models(Forster et al., 2003; Metzler et al., 2006). Thus, we tested retrovirus containing

murine Af4, which is highly conserved with human AF4 (Figure S1E) and observed that virus could be produced at high titers. We therefore constructed a hybrid MLL-Af4 retrovirus that expressed protein corresponding to that found in t(4;11) leukemia cell lines and obtained retroviral titers approximately 30-fold higher than with MLL-AF4 (Figure 1A-C). MLL-Af4 transduction of murine HSPC resulted in immortalization of the cells, not seen using MLL-AF4 (Figure 1D). As a control, we transduced murine HSPC with the N-terminus of MLL. Although high titer virus was produced, only first round colonies were obtained as the N-terminus of MLL by itself was unable to immortalize murine HSPC (Figure 1C and 1D)(Luo et al, 2001). We repeated the experiment using MLL-AF4/-Af4 constructs with the transcriptional activation domain (TAD, also called pSER) truncated (Figure S1A), which corresponds to an MLL-AF4 translocation reported in a patient with a MLL to AF4 exon 11 fusion(Okuda et al., 2015; Pane et al., 2002). Similar to full-length MLL-Af4, MLL-Af4(560-1210) produced high titer virus and immortalized murine HSPC (Figure S1B and S1C). In contrast, MLL-AF4(547-1218) generated low titer virus and did not promote tertiary colony formation, suggesting the titer effect is not associated with the TAD or the specific breakpoint of AF4. To examine whether the difference in retroviral production between MLL-AF4 and MLL-Af4 was a common feature of murine homologs of MLL partners, we prepared fusions of MLL to AF9, Af9, ENL, and Enl. Similar titers were achieved with these human and murine homologs, indicating the difference in virus production is specific to MLL-AF4 (Figure S1D). To assess the leukemogenic potential of MLL-Af4, HSPC were harvested from mice, stimulated with myeloid or lymphoid cytokines (since culture conditions can affect the lineage of the resulting leukemia(Li et al., 1999)), transduced, and transplanted into mice. Mice developed acute leukemia with a median latency of 90 days, manifesting similar disease phenotype irrespective of culture conditions (Figure 1E, Table S1).

Leukemia cells with immature myelomonocytic morphology were observed in bone marrow (BM) and peripheral blood (PB) and expressed c-Kit, Gr-1 and Mac1 but not B220 or CD3 (Figures 1F and 1G). The mice exhibited significant splenomegaly and infiltrating leukemic cells were positive for CD11b and negative for B220 (Figure 1G). Secondary transplant of BM cells confirmed the malignant nature of the disease (Figure 1E). Thus, murine HSPC expressing MLL-Af4 induced AML *in vivo* and, despite the use of lymphoid conditions, no lymphoid leukemia was observed.

Human CD34+ HSPC expressing MLL-Af4 initiate proB ALL in vivo

Murine genetic models of MLL-AF4 leukemia induce primarily AML or lymphoma, and B-ALL is rarely seen (Chen et al., 2006; Krivtsov et al., 2008; Metzler et al., 2006). In contrast, MLL-fusion proteins efficiently induce B-ALL when expressed in human CD34+ cells and transplanted into immunodeficient mice(Barabé et al., 2007; Wei et al., 2008). To test whether MLL-Af4 induces B-ALL in a human model, we transduced human CD34+ cells and injected into NOD/SCID/gamma$^{-/-}$ (NSG) mice. As early as 12 weeks post-transplant, the BM and PB of mice showed an expansion of human CD19+ cells variably expressing CD34 and CD10 (Figure 2A). All animals were leukemic by 22 weeks post-transplant displaying splenomegaly and leukemia infiltration into multiple organs (Figures 2A, 2B and S2A). Analysis by flow cytometry revealed CD19+CD33-CD34+ lymphoid blasts that were predominantly CD10 negative, hallmarks of classic t(4;11) proB ALL (Figures 2A, 2C and S2B)(Burmeister et al., 2009). As reported for t(4;11) patients, the lymphoid blasts expressed the myeloid antigen CD15, although expression of CD65 was less evident compared to patient samples (Figure S2C). Expression of the MLL-Af4 protein was detected in leukemic blasts at physiological levels comparable to

MLL-AF4 in a t(4;11) cell line or patient samples (Figures S2D and S2E). Disease was readily transferred to secondary recipients and showed a similar immunophenotype but with a more predominant CD34+CD10- compartment (Figures 2D and S2F-I). The disease had high penetrance and the phenotype was reproducible in multiple experiments using CD34+ cells from either cord blood or adults (Table S2).

MLL-Af4 proB ALL recapitulates the molecular aspects of t(4;11) disease

Recruitment of the SEC and the H3K79 histone methyltransferase DOT1L is critical for MLL-fusion mediated gene dysregulation and leukemogenesis. Previous work has shown that the mouse Af4 protein harbors this conserved capacity to associate with SEC and DOT1L and stimulate transcription elongation(Bitoun et al., 2007). Accordingly, MLL-Af4 was able to co-immunoprecipitate DOT1L as well as SEC components, exemplified by CDK9 and EAF2, in proB ALL cells (Figure 3A)(Lin et al., 2010; Simone et al., 2003; Yokoyama et al., 2010). The growth of MLL-Af4 cells depended on DOT1L activity and was effectively blocked by a DOT1L inhibitor (Figure 3B). To determine whether MLL-Af4 regulates similar gene targets as MLL-AF4, we performed ChIP-seq analysis of MLL-Af4 in proB ALL cells using anti-FLAG antibody. We compared our results to the ChIP-seq datasets of MLL-AF4 from t(4;11) cell lines SEM and RS4;11, in which the binding loci of MLL-AF4 were determined by the coincident ChIP-seq signals of MLL N-terminus and AF4 C-terminus(Benito et al., 2015; Wilkinson et al., 2013). Heatmaps that rank binding sites according to the strength of either MLL-Af4(FLAG) (Figure 3C) or MLL(N) (Figure S3A) ChIP-seq signal display a clear correlation between the different datasets that are in the range of 70-90% (Figure S3B). Due to the reduced sensitivity of peak-calling algorithms, only 60% of MLL-AF4 peaks in SEM cells were in common with

MLL-Af4 peaks, but this is consistent with the overlap observed between MLL-AF4 peaks in SEM and RS4;11 cells (Figure S3C) and a large number of MLL-Af4 targets overlapped with MLL-AF4 targets in the different cell lines (Figure S3D). Strikingly, at critical MLL-AF4 targets such as MEIS1, RUNX1, FLT3, MYC, BCL2 and PROM1(Benito et al., 2015; Guenther et al., 2008; Wilkinson et al., 2013), the MLL-Af4(FLAG) binding profile is identical to MLL-AF4 in both RS4;11 and SEM cells (Figure 3D and S3E). Accordingly, RNA-Seq analysis of CD19+CD34+ leukemia cells and control human proB cells purified from the BM of NSG mice revealed many MLL-AF4-regulated genes identified in patient samples were also deregulated in MLL-Af4 cells (Figure 3E)(Andersson et al., 2015; Stam et al., 2010). GSEA analysis confirmed significant enrichment of an MLL-AF4 signature (Figure 3F). This data suggests the MLL-Af4 protein retains similar biochemical and molecular properties as the native MLL-AF4 protein. Expression of MLL-Af4 in human CD34+ cells induces proB ALL that mimics the disease found in humans both phenotypically and molecularly. The ability to faithfully recapitulate t(4;11) proB ALL using transduction of human HSPC demonstrates that the proper combination of species of oncogene and targeting cell can serve as an effective approach to overcome difficulties in disease modeling.

Different MLL-fusion proteins cause a different developmental stage block of ALL

Although MLL-fusion induced leukemia has been considered as a single entity, heterogeneity of the disease has been observed(Andersson et al., 2015; Aoki et al., 2015; Stam et al., 2010), suggesting each MLL-fusion protein has its unique characteristics. To test this idea, we performed a comparative analysis of the B-ALL disease induced by MLL-Af4 or MLL-AF9 using matched units of human CD34+ cells. Immunophenotypically, the MLL-AF9-mediated B-

ALL showed variable expression of CD10 and little expression of CD34, suggestive of developmental stage differences (Figure 4A). Transcriptional profiling followed by GSEA analysis showed the MLL-Af4 leukemia resembled a proB developmental stage while the MLL-AF9 B-ALL resembled a preB stage (Figures 4B and 4C)(Hystad et al., 2007). A similar developmental stage difference can be observed when comparing control proB cells with the MLL-AF9 B-ALL but not the MLL-Af4 B-ALL (Figures S4A and S4B). To validate this finding using a published dataset, we compared t(4;11) and t(9;11) ALL patient samples and observed the same differences in B-cell differentiation stage (Figure 4D). It was reported recently that preB cell receptor signaling positive (pre-BCR+) ALL cells rely on different signaling pathways compared to pre-BCR(-) ALL cells(Geng et al., 2015). We tested for pre-BCR status by staining for immunoglobulin u heavy chain (uHC) in our model B-ALL samples and found positivity on MLL-AF9 but not MLL-Af4 B-ALL cells (Figure S4C). BCL6 expression is a surrogate maker of pre-BCR signaling(Geng et al., 2015), and in accordance with this fact, the model MLL-AF9 ALL cells had significantly higher BCL6 expression compared to MLL-Af4, which was also seen in patient samples (Figure S4D). These findings again demonstrate the unique molecular features driving the differential phenotype of the two MLL-fusion leukemias.

MLL-Af4 drives a gene expression profile distinct from MLL-AF9 through binding to different genomic targets

In addition to immunophenotypic differences, heterogeneous gene expression profiles of MLL-fusion ALL were also observed. A recent study identified the top 100 genes that best discriminate different MLL-fusion B-ALL according to specific translocation partner(Andersson et al., 2015). Unsupervised hierarchical clustering based on these 100 genes demonstrated the

fidelity of our MLL-Af4 and MLL-AF9 model leukemias, with each leukemia associating closely with the respective patient samples (Figures 5A and 5B). In addition, based on the expression of genes significantly differentially expressed between our MLL-Af4 and MLL-AF9 ALL, t(4;11) patient samples clustered closely with MLL-Af4 cells and were readily distinguished from other MLL-fusion samples (Figures S5A and S5B). We examined the expression profiles for gene families that distinguish MLL-Af4 and MLL-AF9 B-ALL and identified the *HOXA* cluster as significantly differentially expressed (Figure 5C). *HOXA9* is considered a bona fide downstream target and one of most critical mediators in MLL-fusion AML(Faber et al., 2009). However, recent analyses showed that approximately half of t(4;11) ALL patients do not have an activated *HOXA* signature(Stam et al., 2010; Trentin et al., 2009). In our model system, MLL-Af4 ALL do not upregulate *HOXA* genes compared to control proB cells, in stark contrast to MLL-AF9 ALL (Figures 5C and 5D). By comparison, *MEIS1*, another well-known target of MLL-fusions, is equally expressed in both types of leukemia, and *RUNX1*, a key target in t(4;11) leukemogenesis(Wilkinson et al., 2013), is specifically increased only in MLL-Af4 ALL (Figure 5D). Given that our ALL cells have matched genetic backgrounds, this suggests that the unique fusion protein is the major driving force behind differential gene expression. Although the DNA binding properties of the different MLL-fusion proteins remain poorly understood, the presumption in the field is that the fusion proteins are targeted to gene loci via the DNA binding domains of MLL, and thus have similar DNA binding profiles. However, we have shown that MLL-fusion proteins only bind to a subset of wildtype MLL targets(Wang et al., 2011), suggesting that the translocation partner genes alter and modify the fusion protein's binding properties. To test whether distinct chromatin binding abilities of different MLL-fusions serves as a molecular mechanism driving heterogeneous gene expression,

we performed ChIP-qPCR to compare the chromatin occupancy of MLL-Af4 and MLL-AF9 at these specific loci. Indeed, chromatin occupancy correlated with gene expression, with no binding of MLL-Af4 at the *HOXA* locus and no MLL-AF9 binding at the *RUNX1* locus (Figure 5E). Several additional differentially-expressed MLL-Af4 and -AF9 genes were also found to correlate with specific chromatin binding of the different MLL-fusion proteins (Figure S6). These results demonstrate that differential target region recognition of MLL-fusion proteins contributes to distinct gene expression profiles.

MLL-Af4 myeloid cells retain lymphoid lineage potential

While the tight association of t(4;11) with proB-cell ALL is well known, the explanation for this pathologic phenotype, i.e. a specific target cell type versus a distinct epigenetic reprogramming activity leading towards a B-cell fate, has been unclear. We and others have previously shown that human CD34+ cells expressing MLL-AF9 generate AML in immunodeficient mice after priming in myeloid culture conditions (Barabé et al., 2007; Goyama et al., 2015; Wei et al., 2008). Surprisingly, myeloid cultures expressing MLL-Af4 retained a population of CD19+CD33- cells not present in paired MLL-AF9 cultures (Figure S7A). When cells were transferred to B-lymphoid promoting conditions, CD19+CD33- cells rapidly expanded in MLL-Af4 but not MLL-AF9 cultures (Figure 6A). Similarly, upon injection into NSG mice, the MLL-Af4 myeloid cells reproducibly induced human B-ALL with a CD34+CD10- proB cell phenotype, while the MLL-AF9 cells invariably gave CD33+CD19- AML (Figures 6B and S7B). B-ALL also developed upon injection of MLL-Af4 myeloid cultures containing no detectable CD19+ cells (Figures S7C and S7D). Moreover, sorted CD33+CD19- MLL-Af4 cells reproducibly generated CD33-CD19+ B-lymphoid cells under B-cell growth conditions (Figure

6C), indicating the CD33+CD19- MLL-Af4 cells harbor latent B-cell potential refractory to myeloid priming. MLL-Af4 cells derived from adult CD34+ cells showed identical lymphoid persistence as CD34+ cells obtained from cord blood (data not shown), in contrast to data showing MLL leukemia lineage is ontogenically determined, with AML resulting from adult-origin and ALL from fetal-origin HSPC(Horton et al., 2013), These results suggest that lymphoid preference is an MLL-Af4 intrinsic property that overrides the lineage instruction from the microenvironment and the influence of cell-of-origin. RNA-Seq analysis of sorted CD33+CD19- cells from four sets of genetically matched MLL-Af4 or MLL-AF9 myeloid cultures showed uniform upregulation of key B-lymphoid genes and a decrease in specific myeloid genes in MLL-Af4 cells compared to matched MLL-AF9 cells, demonstrating that MLL-Af4 transduced cells maintain an active lymphoid program responsible for the B-cell bias of human disease (Figures 6D and S7E).

t(4;11) ALL acquires resistance to CD19-targeted therapy by myeloid differentiation

A recent treatment advance in relapsed B-ALL employs a bispecific antibody, blinatumomab, that specifically targets CD19 on B cells(Topp et al., 2011). In a pediatric patient with refractory t(4:11) proB ALL treated with blinatumomab, t(4;11) AML relapse was observed (Figures 7A and 7B)(Rayes et al., 2016). These t(4;11) myeloid cells promoted B-ALL in NSG mice, even when using sorted CD33+CD19- cells (Figure 7C). A marker chromosome indicated the B-ALL cells that expanded in the mouse were clonally related to the initial myelomonocytic cells (data not shown). QPCR analysis of this AML in comparison to standard AML samples showed significant upregulation of some of the same B-cell genes identified in the MLL-Af4 cells (Figure 7D). Thus similar to the effects seen with the MLL-Af4 myeloid cultures, a persistent

lymphoid program resistant to environmental induction and resulting in potent B-lymphoid preference is associated with the t(4;11) fusion protein, showing the utility of our MLL-Af4 model system as applied to clinical disease. We also identified an adult patient with t(4;11) proB ALL treated with blinatumomab who relapsed with morphologic, cytochemical, and immunophenotypic evidence of differentiation towards the monocytic lineage (Figures 7E-7G). This phenotypic flexibility represents a novel escape mechanism from CD19-targeted treatment for patients with t(4:11) ALL, and has also been reported recently in t(4;11) patients receiving chimeric antigen receptor T-cell (CAR-T) therapies directed against CD19(Gardner et al., 2016). Therapeutic strategies may need to be customized for this poor prognosis leukemia showing phenotypic plasticity with transcriptional lymphoid persistence under selective pressure of CD19-directed therapy. Our model accurately recapitulates both a de novo ALL stage and a refractory 'AML' stage, enabling studies to proceed that may reveal new insights into molecular mechanisms and permit development of novel therapies.

Discussion

Chromosomal rearrangements involving 11q23 replace the C-terminus of MLL with more than 79 different fusion partner proteins(Meyer et al., 2013) raising the question of the molecular mechanism of action of the different fusion partners and their relevance for leukemia biology. As MLL-AF4 is the most frequently observed MLL-fusion protein, significant efforts have been devoted to generating a suitable mouse model that recapitulates the full spectrum of human disease and generates a proB ALL (Bueno et al., 2012; Bursen et al., 2010; Chen et al., 2006; Krivtsov et al., 2008; Metzler et al., 2006; Montes et al., 2011). The inability to generate a faithful model of MLL-AF4 leukemia has led to the hypotheses that MLL-AF4 is unable to

transform cells without cooperating oncogenes, that an alternative cell of origin is needed, or that the reciprocal fusion is the true driver of leukemogenesis(Bursen et al., 2010; Menendez et al., 2009; Tamai et al., 2011). Our results demonstrate that, at least for MLL-Af4 driven B-ALL, prehematopoietic mesodermal or hemangioblast precursors are not required as initiating cells and the reciprocal AF4-MLL-fusion is dispensable. Whether these observations hold true in t(4;11) patients remains to be determined.

We and others have previously observed very low retroviral titers from producer cells expressing MLL-AF4 which precluded the analysis of its effects on virally transduced murine and human HSPCs(Bursen et al., 2010; Montes et al., 2011; Yokoyama et al., 2010). Experiments from several labs have shown that the titer obtained is critical to the efficiency of retroviral infection rather than the number of target cells, with only high titer retrovirus capable of efficient gene transfer into cells (Bodine et al., 1990; Haas et al., 2000; Morgan et al., 1995). Although the mouse and human AF4 proteins are highly conserved, distinct species-related differences in the viral titer are achieved using mouse Af4 and human AF4 cDNAs. This effect is specific to AF4 as we did not observe differences in retroviral titer between the human and murine homologs of AF9 or ENL. Truncation of the TAD/pSER domain of AF4 did not rescue the low titers of retrovirus observed with MLL-AF4, indicating that these sequences do not inhibit the production of retrovirus. Although the smaller size of the *MLL-AF4*(560-1210) cDNA would be predicted to permit higher packaging efficiency, we observed only a minimal increase in titer with this construct, indicating that size is not the cause of the low retroviral titers generated with MLL-AF4.. The reason for low viral titer production by retroviral vectors containing human AF4 is not clear. Certain human cDNA sequences have been found to have significant effects on retroviral titer formation(Skalamera et al., 2012). For some cDNAs, the mechanism that prevents virus

production has been identified. In the case of human IL-1 receptor antagonist protein, a cryptic splice acceptor sequence was found to be present in the middle of its coding region resulting in the deletion of the packaging signal sequence and the removal of some coding sequences that lead to low viral titer and a low level of the transgene product (Lee et al., 2007). For other cDNAs, the mechanisms that affect titer are unclear but have been mapped. For example, the positioning of the v-src gene relative to the tk gene in a retroviral vector was found to give a 30-fold difference in retroviral titer (Tarpley et al. 1984). Other factors have been reported including inhibitory sequences affecting nucleic acid sequence-dependent steps in virus production, inappropriate signals present in some sequences that inhibit virus production, and potential toxic effects of the gene sequence on producer cells (Swift et al., 2001). Inspired by these observations, we fused human MLL to murine Af4 and achieved a significant increase in retroviral titer thus permitting efficient transduction of HSPC.

While MLL-Af4 efficiently transformed murine HSPC and induced leukemia, mice developed only AML. Strikingly, AML is the primary phenotype observed in Mll-AF4 knock-in mice, indicating that the MLL-Af4 fusion results in a similar phenotype to Mll-AF4 when expressed in murine HSPCs(Kristov et al., 2008). Similarly, mouse models of E2A-PBX1, a fusion oncoprotein associated exclusively with human preB ALL, have also resulted in the unexpected generation of myeloid leukemia. (Kamps and Baltimore, 1993). In stark contrast, expression of MLL-Af4 in human CD34+ cells faithfully recapitulates the proB ALL observed in patients with the t(4:11) as shown by immunophenotype, chromatin targeting of the fusion, nuclear complex formation and gene expression signatures. The factors that mediate myeloid lineage preference of E2A-PBX1 and MLL-Af4 in murine cells remain unknown, highlighting the limitation of using mouse cells for modeling human disease.

Proteins that are frequently part of MLL translocations were identified as components of the SEC (Lin et al., 2010) and are involved in complex interactions with the H3K79 histone methyltransferase DOT1L (Yokoyama et al., 2010). Aberrant transcriptional elongation and H3K79 methylation lead to aberrant activation of common target genes such as *HOXA* and *MEIS1* and are considered a general mechanism of MLL-fusion mediated leukemogenesis. Indeed, a shared transcriptional signature with *HOXA* upregulation has been identified for MLL-fusion leukemia irrespective of fusion partner or lineage(Armstrong et al., 2002). However, biological differences observed when studying subtypes of MLL-fusion leukemia raise questions regarding these findings. For instance, *FLT3*, which is regarded as a general MLL-fusion target, is required for MLL-ENL but not MLL-AF9 AML (Kamezaki et al., 2014). The necessity of *HOXA* activation has also been challenged, as it was shown that *Hoxa9* is dispensable for leukemia development in murine MLL-AF9 and MLL-GAS7 AML models (Kumar et al., 2004; So et al., 2004). Moreover, 50% of t(4;11) ALL patients do not show *HOXA* gene activation, and low *HOXA* gene expression is actually associated with a poor prognosis(Stam et al., 2010; Trentin et al., 2009). Instead, it has been suggested that MLL-fusions can activate alternative pathways for leukemia development, such as *RUNX1*(Wilkinson et al., 2013). Our data show that MLL-Af4 ALL cells do not have increased *HOXA* expression relative to normal proB cells, but that MLL-Af4 does bind to the RUNX1 promoter and activates expression (Figures 5C-E). These results indicate that at least for one set of MLL-fusion ALL, activation of *HOXA* is not required for leukemogenesis.

Although a common gene expression signature was identified for MLL-fusion leukemia, significant fusion partner transcriptome and DNA methylome heterogeneity has been found

(Andersson et al., 2015; Stam et al., 2010; Stumpel et al., 2011). The mechanisms accounting for this heterogeneity are not fully understood partly due to difficulties of working with limited numbers of leukemia cells and the confounding complex genetic backgrounds in patient samples. We show here that fusion proteins are truly instructive since matched MLL-Af4 and MLL-AF9 ALL cells with the same genetic background can recapitulate the fusion partner specific gene signature derived from patient samples (Figures 5A and 5B). In addition, the signature generated from our model leukemia can be utilized to classify patient samples (Figure S5). Importantly, we demonstrate that diverse target recognition of different fusion proteins is one molecular mechanism controlling differential gene regulation (Figure 5E and S6) implicating the fusion partners in this function, potentially through recruitment of distinct protein partners as reported previously(Lin et al., 2010). Therefore, our data questions the idea that all MLL-fusion proteins work in a similar fashion by dysregulating the same pathways and demonstrates that MLL-fusion leukemia represents a heterogeneous disease.

The instructive role of the fusion partner in lineage determination of the disease has been reported previously(Barabé et al., 2007; Drynan et al., 2005; Wei et al., 2008). Here we show that even within the same lineage, different MLL-fusion partner proteins enforce a block at distinct stages of differentiation whereby MLL-Af4 ALL cells display a proB immunophenotype and MLL-AF9 ALL cells resemble a later preB stage (Figures 4, S4A and S4B). Moreover, MLL-AF9 cells express both surface and cytoplasmic uHC, suggesting they have active pre-BCR signaling (Figure S4C). A recent report showed that pre-BCR+ ALL is a distinct subtype from pre-BCR(-) ALL, relying on a different signaling pathway and showing a selective sensitivity to pre-BCR tyrosine kinase inhibitors(Geng et al., 2015). Our data show that MLL-AF4 and MLL-AF9 leukemia may also depend on diverse signaling pathways adding weight to

the idea that therapeutic targets identified in one MLL subtype may not be applicable to others and customized therapies may need to be established for each disease.

In patients, MLL-AF4 is almost exclusively associated with B-ALL, while MLL-AF9 is more common in AML(Meyer et al., 2013). In line with the instructive role of the fusion partner, this different lineage association is also recapitulated in our comparative studies, reflected by the fact that MLL-Af4 cells are resistant to environmental myeloid redirection and maintain a persistently active lymphoid program (Figures 6 and S7). While MLL-AF9 cells acquire a stable myeloid fate after myeloid priming and give rise to AML, MLL-Af4 cells return to a lymphoid fate once the environmental pressure is released. Strikingly, this assumed myeloid status appears to be a novel mechanism for t(4;11) disease to escape from blinatumomab therapy (Figure 7), and possibly for the development of resistance to other CD19-directed immunotherapies, such as CAR-T therapy(Gardner et al., 2016). Clinically, how these myeloid cells with lymphoid potential respond to traditional AML therapy compared to conventional AML cells is unknown. Our MLL-Af4 myeloid cultures will be useful to evaluate drug sensitivity for eliminating resistant disease.

In summary, our results and correlating observations in patients demonstrate that MLL-fusion disease is not a single genetic entity. Although different MLL-fusion proteins share some common properties, each has its own genetic and biologic features associated with particular fusion partner proteins. These differences could potentially impact response to therapy. Our MLL-Af4 model will be a valuable tool to study this most prevalent and poor prognosis MLL-fusion leukemia.

Author Contributions

SL, RTL, JCM and MJT conceived and designed the study, analyzed data and wrote the

manuscript. CB and TAM helped edit the manuscript and analyzed data. SL, RTL, JJK, TI, MW, MJA, and JA performed experiments. AP and ARM performed experiments and analyzed data. JK, and SAA analyzed data. AR and MMO analyzed patient samples.

Acknowledgements

We thank G. Huang, A. Kumar, M. Azam and members of the Mulloy and Thirman laboratories for reagents, experimental assistance and feedback. This work was supported by an Institutional Clinical and Translational Science Award, NIH/NCRR Grant Number 1UL1RR026314-01, Translational Trials Development and Support Laboratory award (U.S.P.H.S. Grant Number MO1 RR 08084), a Center of Excellence in Molecular Hematology P30 award (DK090971), a CancerFree KIDS Research Award (SL), an American Society of Hematology Bridge Grant (MJT), a Leukemia and Lymphoma Society Translational Research Grant (MJT), a Leukemia and Lymphoma Society Scholar award (JCM), grants from Bloodwise and the Kay Kendall Leukaemia Fund (CB), the assistance of the CCHMC Research Flow Cytometry Core, CCHMC Translational Core Laboratory, CCHMC Pathology Core and CCHMC Comprehensive Mouse and Cancer Core, Genomics, Epigenomics and Sequencing Core (NIEHS P30-ES006096), the sequencing facility of the University of Birmingham (UK) and Statistical Genomics and Systems Biology Core at the University of Cincinnati, and the Genomics Core and the Cytometry and Antibody Technology Core of the University of Chicago. TAM and JK are supported by a Medical Research Council (MRC, UK) Molecular Haematology Unit grant MC_UU_12009/6. TAM is one of the founding shareholders of Oxstem Oncology (OSO), a subsidiary company of OxStem Ltd (2016).

Experimental Procedures

Cells and culture

Patient samples were acquired following informed consent in accordance with the Declaration of Helsinki and under protocols approved by the institutional review board. Human umbilical cord blood cells (CB) or adult PB progenitor cells (PBPC) were obtained by the Translational Trials Support Laboratory at CCHMC under an approved protocol. CD34+ cells were enriched using CD34+ selection kit (Miltenyi). Details of culture conditions are in Supplemental Experimental Procedures.

Retroviral production

AF4, Af4, AF9, Af9, ENL, and Enl cDNAs were ligated to 5' MLL and cloned in the MSCV retroviral vector. An in-frame FLAG tag was inserted between MLL residue 1404 (in exon 11) and the beginning of the partner protein sequence. Retrovirus for transduction of murine cells was packaged in Phoenix cells as described(Luo et al., 2001). Viral titers were determined by infection of Rat1A cells with Phoenix retroviral supernatants followed by selection in G418. Virus for human cell transduction was produced using 293T cells transfected with MSCV-MLL-fusion vectors, together with envelope RD114 and the gag-pol M57 constructs in 10 cm plates. 24 h after transfection, the retroviral supernatant were collected every 12h for 3 collections.

Mouse transplantation

Transplantation was performed using both myeloid and lymphoid conditions. For the myeloid reconstitution assays, 6 week old C57/BL6 mice were pretreated with 5- fluorouracil at 150 mg/kg by intravenous injection and BM cells were harvested 5 days later. Lin- cells were selected using columns (Miltenyi) and cultured in RPMI media containing β-mercaptoethanol 0.05mM, 10% FBS supplemented with 100 ng/ml SCF, 10 ng/ml IL-3, and 10 ng/ml IL-6 (R&D

Systems, Minneapolis, MN). For the lymphoid conditions, Lin- BM cells were harvested from 6 week old C57/BL6 mice without 5- fluorouracil pretreatment. Lin- BM cells were cultured in 100 ng/ml SCF, 10 ng/ml IL-7, 10 ng/ml IL-6, and Flt-3 ligand 10 ng/ml (R&D Systems) (Li et al, 1999). Reconstitution of sub-lethally irradiated C57BL/6 mice with transduced progenitors was performed as described previously (Luo et al., 2001). Further details of transduction, transplantation and histological analysis are in Supplemental Experimental Procedures.

Xenograft transplantation

500K CD34+cells were used for each transduction. CD34+ cells were pre-stimulated in IMDM with 10%FBS, SCF, FLT3L, and TPO (100ng/mL) for 24 h. Retronectin-coated plates were preloaded three times with 3mL retroviral supernatant by centrifuging at 2200rpm and 10°C for 25 min. Stimulated cells were cultured in the presence of 3mL retroviral supernatant on virus-loaded plates (Takara) overnight, 3mL fresh retroviral supernatant was replaced, and cells were cultured for another 6 h. To induce acute leukemia in NSG mice, 6- to 12-week-old mice were conditioned with 30mg/kg busulfan (Sigma) through intraperitoneal injection 24 h before transplantation, 100-150K MLL-Af4 or -AF9 transduced cells were transplanted through intrafemoral injection immediately after transduction. Mice were sacrificed when signs of illness were observed. Organs were homogenized and processed for flow cytometry or fixed in 10% formalin for histopathologic analysis. In serial transplantation, 1M BM cells were injected through tail vein. Further details of transplantation are in Supplemental Experimental Procedures.

Chromatin immunoprecipitation (ChIP)

MLL-Af4 and -AF9 ALL cells were harvested from mice BM and spleen and subjected for ChIP. The ChIP assay was performed as described previously (Ptasinska et al., 2014). Details of

protocols used for ChIP-qPCR, ChIP-seq and data analyses are in Supplemental Experimental Procedures.

RNA isolation and RNA sequencing

Human CD45+ CD19+ cells were sorted from BM of 6 individual MLL-Af4 (3 PBPC based and 3 CB based, generated by 2 independent transduction) and 3 individual MLL-AF9 (CB based, generated by one transductions) leukemic mice. For control proB cells, non-transduced CD34+ CB cells were transplanted into NSG mice, human CD45+CD19+CD34+ proB cells were sorted from BM of 3 mice 8 weeks later. For myeloid-primed culture study, CD33+CD19- cells were sorted from 4 pairs of MLL-Af4 and -AF9 clones (2 PBPC based and 2 CB based, generated by 4 independent transductions) that had been cultured in myeloid conditions for 6-8 weeks. Patient samples were similarly sorted. Total RNA was isolated from sorted cells using RNeasy Mini Kit (Qiagen).

For RNA sequencing, the integrity of RNA was analyzed by Bioanalyzer (Agilent). RNA from each individual mouse was processed separately without pooling. Details of protocols used for RT-PCR, RNA sequencing and data analyses are in Supplemental Experimental Procedures.

Data access

RNA-Seq and ChIP-seq datasets are deposited to GEO as GSE76978 and GSE84116, respectively.

References

Andersson, A. K., Ma, J., Wang, J., Chen, X., Gedman, A. L., Dang, J., Nakitandwe, J., Holmfeldt, L., Parker, M., Easton, J.*, et al.* (2015). The landscape of somatic mutations in infant MLL-rearranged acute lymphoblastic leukemias. Nat Genet *47*, 330-337.

Aoki, Y., Watanabe, T., Saito, Y., Kuroki, Y., Hijikata, A., Takagi, M., Tomizawa, D., Eguchi, M., Eguchi-Ishimae, M., Kaneko, A.*, et al.* (2015). Identification of CD34+ and CD34- leukemia-initiating cells in MLL-rearranged human acute lymphoblastic leukemia. Blood *125*, 967-980.

Armstrong, S. a., Staunton, J. E., Silverman, L. B., Pieters, R., den Boer, M. L., Minden, M. D., Sallan, S. E., Lander, E. S., Golub, T. R., and Korsmeyer, S. J. (2002). MLL translocations specify a distinct gene expression profile that distinguishes a unique leukemia. Nat Genet *30*, 41-47.

Barabé, F., Kennedy, J. a., Hope, K. J., and Dick, J. E. (2007). Modeling the initiation and progression of human

acute leukemia in mice. Science (New York, NY *316*, 600-604.
Benito, J. M., Godfrey, L., Kojima, K., Hogdal, L., Wunderlich, M., Geng, H., Marzo, I., Harutyunyan, K. G., Golfman, L., North, P.*, et al.* (2015). MLL-Rearranged Acute Lymphoblastic Leukemias Activate BCL-2 through H3K79 Methylation and Are Sensitive to the BCL-2-Specific Antagonist ABT-199. Cell Rep *13*, 2715-2727.
Bitoun, E., Oliver, P. L., and Davies, K. E. (2007). The mixed-lineage leukemia fusion partner AF4 stimulates RNA polymerase II transcriptional elongation and mediates coordinated chromatin remodeling. Hum Mol Genet *16*, 92-106.
Bodine, D. M., McDonagh, K. T., Brandt, S. J., Ney, P. A., Agricola, B., Byrne, E., and Nienhuis, A. W. (1990). Development of a high-titer retrovirus producer cell line capable of gene transfer into rhesus monkey hematopoietic stem cells. Proc Natl Acad Sci U S A *87*, 3738-3742.
Bueno, C., Montes, R., Melen, G. J., Ramos-Mejia, V., Real, P. J., Ayllon, V., Sanchez, L., Ligero, G., Gutierrez-Aranda, I., Fernandez, A. F.*, et al.* (2012). A human ESC model for MLL-AF4 leukemic fusion gene reveals an impaired early hematopoietic-endothelial specification. Cell Res *22*, 986-1002.
Burmeister, T., Meyer, C., Schwartz, S., Hofmann, J., Molkentin, M., Kowarz, E., Schneider, B., Raff, T., Reinhardt, R., Gökbuget, N.*, et al.* (2009). The MLL recombinome of adult CD10-negative B-cell precursor acute lymphoblastic leukemia: Results from the GMALL study group. Blood *113*, 4011-4015.
Bursen, A., Schwabe, K., Ruster, B., Henschler, R., Ruthardt, M., Dingermann, T., and Marschalek, R. (2010). The AF4.MLL fusion protein is capable of inducing ALL in mice without requirement of MLL.AF4. Blood *115*, 3570-3579.
Chen, W., Li, Q., Hudson, W. A., Kumar, A., Kirchhof, N., and Kersey, J. H. (2006). A murine Mll-AF4 knock-in model results in lymphoid and myeloid deregulation and hematologic malignancy. Blood *108*, 669-677.
Drynan, L. F., Pannell, R., Forster, A., Chan, N. M., Cano, F., Daser, A., and Rabbitts, T. H. (2005). Mll fusions generated by Cre-loxP-mediated de novo translocations can induce lineage reassignment in tumorigenesis. EMBO J *24*, 3136-3146.
Faber, J., Krivtsov, A. V., Stubbs, M. C., Wright, R., Davis, T. N., van den Heuvel-Eibrink, M., Zwaan, C. M., Kung, A. L., and Armstrong, S. A. (2009). HOXA9 is required for survival in human MLL-rearranged acute leukemias. Blood *113*, 2375-2385.
Forster, A., Pannell, R., Drynan, L. F., McCormack, M., Collins, E. C., Daser, A., and Rabbitts, T. H. (2003). Engineering de novo reciprocal chromosomal translocations associated with Mll to replicate primary events of human cancer. Cancer Cell *3*, 449-458.
Gardner, R., Wu, D., Cherian, S., Fang, M., Hanafi, L. A., Finney, O., Smithers, H., Jensen, M. C., Riddell, S. R., Maloney, D. G., and Turtle, C. J. (2016). Acquisition of a CD19 negative myeloid phenotype allows immune escape of MLL-rearranged B-ALL from CD19 CAR-T cell therapy. Blood.
Geng, H., Hurtz, C., Lenz, K. B., Chen, Z., Baumjohann, D., Thompson, S., Goloviznina, N. A., Chen, W. Y., Huan, J., LaTocha, D.*, et al.* (2015). Self-enforcing feedback activation between BCL6 and pre-B cell receptor signaling defines a distinct subtype of acute lymphoblastic leukemia. Cancer Cell *27*, 409-425.
Goyama, S., Wunderlich, M., and Mulloy, J. C. (2015). Xenograft models for normal and malignant stem cells. Blood *125*, 2630-2641.
Guenther, M. G., Lawton, L. N., Rozovskaia, T., Frampton, G. M., Levine, S. S., Volkert, T. L., Croce, C. M., Nakamura, T., Canaani, E., and Young, R. A. (2008). Aberrant chromatin at genes encoding stem cell regulators in human mixed-lineage leukemia. Genes Dev *22*, 3403-3408.
Haas, D. L., Case, S. S., Crooks, G. M., and Kohn, D. B. (2000). Critical factors influencing stable transduction of human CD34(+) cells with HIV-1-derived lentiviral vectors. Mol Ther *2*, 71-80.
Horton, S. J., Jaques, J., Woolthuis, C., van Dijk, J., Mesuraca, M., Huls, G., Morrone, G., Vellenga, E., and Schuringa, J. J. (2013). MLL-AF9-mediated immortalization of human hematopoietic cells along different lineages changes during ontogeny. Leukemia *27*, 1116-1126.
Hystad, M. E., Myklebust, J. H., Bo, T. H., Sivertsen, E. A., Rian, E., Forfang, L., Munthe, E., Rosenwald, A., Chiorazzi, M., Jonassen, I.*, et al.* (2007). Characterization of early stages of human B cell development by gene expression profiling. J Immunol *179*, 3662-3671.
Kalberer, C. P., Antonchuk, J., and Keith Humphries, R. (2002). Genetic modification of murine hematopoietic stem cells by retroviruses. Methods Mol Med *63*, 231-242.
Kamezaki, K., Luchsinger, L. L., and Snoeck, H.-W. (2014). Differential requirement for wild-type Flt3 in leukemia initiation among mouse models of human leukemia. Exp Hematol *42*, 192-203.e191.
Kamps, M. P., and Baltimore, D. (1993). E2A-Pbx1, the t(1;19) translocation protein of human pre-B-cell acute lymphocytic leukemia, causes acute myeloid leukemia in mice. Mol Cell Biol *13*, 351-357.
Krivtsov, A. V., Feng, Z., Lemieux, M. E., Faber, J., Vempati, S., Sinha, A. U., Xia, X., Jesneck, J., Bracken, A. P.,

Silverman, L. B.*, et al.* (2008). H3K79 Methylation Profiles Define Murine and Human MLL-AF4 Leukemias. Cancer Cell *14*, 355-368.
Kumar, A. R., Hudson, W. A., Chen, W., Nishiuchi, R., Yao, Q., and Kersey, J. H. (2004). Hoxa9 influences the phenotype but not the incidence of Mll-AF9 fusion gene leukemia. Blood *103*, 1823-1828.
Lavau, C., Szilvassy, S. J., Slany, R., and Cleary, M. L. (1997). Immortalization and leukemic transformation of a myelomonocytic precursor by retrovirally transduced HRX-ENL. EMBO J *16*, 4226-4237.
Li, S., Ilaria, R. L., Million, R. P., Daley, G. Q., and Van Etten, R. A. (1999). The P190, P210, and P230 forms of the BCR/ABL oncogene induce a similar chronic myeloid leukemia-like syndrome in mice but have different lymphoid leukemogenic activity. The Journal of experimental medicine *189*, 1399-1412.
Lin, C., Smith, E. R., Takahashi, H., Lai, K. C., Martin-Brown, S., Florens, L., Washburn, M. P., Conaway, J. W., Conaway, R. C., and Shilatifard, A. (2010). AFF4, a component of the ELL/P-TEFb elongation complex and a shared subunit of MLL chimeras, can link transcription elongation to leukemia. Mol Cell *37*, 429-437.
Liu, H., Westergard, T. D., Cashen, A., Piwnica-Worms, D. R., Kunkle, L., Vij, R., Pham, C. G., DiPersio, J., Cheng, E. H., and Hsieh, J. J. (2014). Proteasome inhibitors evoke latent tumor suppression programs in Pro-B MLL Leukemias through MLL-AF4. Cancer Cell *25*, 530-542.
Luo, R. T., Lavau, C., Du, C., Simone, F., Polak, P. E., Kawamata, S., and Thirman, M. J. (2001). The elongation domain of ELL is dispensable but its ELL-associated factor 1 interaction domain is essential for MLL-ELL-induced leukemogenesis. Mol Cell Biol *21*, 5678-5687.
Marchesi, F., Girardi, K., and Avvisati, G. (2011). Pathogenetic, Clinical, and Prognostic Features of Adult t(4;11)(q21;q23)/MLL-AF4 Positive B-Cell Acute Lymphoblastic Leukemia. Adv Hematol *2011*, 621627.
Menendez, P., Catalina, P., Rodriguez, R., Melen, G. J., Bueno, C., Arriero, M., Garcia-Sanchez, F., Lassaletta, A., Garcia-Sanz, R., and Garcia-Castro, J. (2009). Bone marrow mesenchymal stem cells from infants with MLL-AF4+ acute leukemia harbor and express the MLL-AF4 fusion gene. J Exp Med *206*, 3131-3141.
Metzler, M., Forster, A., Pannell, R., Arends, M. J., Daser, A., Lobato, M. N., and Rabbitts, T. H. (2006). A conditional model of MLL-AF4 B-cell tumourigenesis using invertor technology. Oncogene *25*, 3093-3103.
Meyer, C., Hofmann, J., Burmeister, T., Gröger, D., Park, T. S., Emerenciano, M., Pombo de Oliveira, M., Renneville, a., Villarese, P., Macintyre, E.*, et al.* (2013). The MLL recombinome of acute leukemias in 2013. Leukemia *27*, 2165-2176.
Montes, R., Ayllon, V., Gutierrez-Aranda, I., Prat, I., Hernandez-Lamas, M. C., Ponce, L., Bresolin, S., Te Kronnie, G., Greaves, M., Bueno, C., and Menendez, P. (2011). Enforced expression of MLL-AF4 fusion in cord blood CD34+ cells enhances the hematopoietic repopulating cell function and clonogenic potential but is not sufficient to initiate leukemia. Blood *117*, 4746-4758.
Morgan, J. R., LeDoux, J. M., Snow, R. G., Tompkins, R. G., and Yarmush, M. L. (1995). Retrovirus infection: effect of time and target cell number. J Virol *69*, 6994-7000.
Okuda, H., Kanai, A., Ito, S., Matsui, H., and Yokoyama, A. (2015). AF4 uses the SL1 components of RNAP1 machinery to initiate MLL fusion- and AEP-dependent transcription. Nat Commun *6*, 8869.
Pane, F., Intrieri, M., Izzo, B., Quintarelli, C., Vitale, D., Migliorati, R., Sebastio, L., and Salvatore, F. (2002). A novel MLL/AF4 fusion gene lacking the AF4 transactivating domain in infant acute lymphoblastic leukemia. Blood *100*, 4247-4248.
Ptasinska, A., Assi, S. A., Martinez-Soria, N., Imperato, M. R., Piper, J., Cauchy, P., Pickin, A., James, S. R., Hoogenkamp, M., Williamson, D.*, et al.* (2014). Identification of a dynamic core transcriptional network in t(8;21) AML that regulates differentiation block and self-renewal. Cell Rep *8*, 1974-1988.
Rayes, A., McMasters, R. L., and O'Brien, M. M. (2016). Lineage Switch in MLL-Rearranged Infant Leukemia Following CD19-Directed Therapy. Pediatric blood & cancer *63*, 1113-1115.
Simone, F., Luo, R. T., Polak, P. E., Kaberlein, J. J., and Thirman, M. J. (2003). ELL-associated factor 2 (EAF2), a functional homolog of EAF1 with alternative ELL binding properties. Blood *101*, 2355-2362.
Skalamera, D., Dahmer, M., Purdon, A. S., Wilson, B. M., Ranall, M. V., Blumenthal, A., Gabrielli, B., and Gonda, T. J. (2012). Generation of a genome scale lentiviral vector library for EF1alpha promoter-driven expression of human ORFs and identification of human genes affecting viral titer. PLoS One *7*, e51733.
So, C. W., Karsunky, H., Wong, P., Weissman, I. L., and Cleary, M. L. (2004). Leukemic transformation of hematopoietic progenitors by MLL-GAS7 in the absence of Hoxa7 or Hoxa9. Blood *103*, 3192-3199.
Stam, R. W., Schneider, P., Hagelstein, J. a. P., Van Der Linden, M. H., Stumpel, D. J. P. M., De Menezes, R. X., De Lorenzo, P., Valsecchi, M. G., and Pieters, R. (2010). Gene expression profiling-based dissection of MLL translocated and MLL germline acute lymphoblastic leukemia in infants. Blood *115*, 2835-2844.
Stumpel, D. J. P. M., Schneider, P., Roon, E. H. J. V., Boer, J. M., De, P., Valsecchi, M. G., Menezes, R. X. D., Pieters, R., Stam, R. W., Dc, W., and Lorenzo, P. D. (2011). Specific promoter methylation identifies different

subgroups of MLL-rearranged infant acute lymphoblastic leukemia, influences clinical outcome, and provides therapeutic options. Blood *114*, 5490-5498.
Swift, S., Lorens, J., Achacoso, P., and Nolan, G. P. (2001). Rapid production of retroviruses for efficient gene delivery to mammalian cells using 293T cell-based systems. Curr Protoc Immunol *Chapter 10*, Unit 10 17C.
Tamai, H., Miyake, K., Takatori, M., Miyake, N., Yamaguchi, H., Dan, K., Shimada, T., and Inokuchi, K. (2011). Activated K-Ras protein accelerates human MLL/AF4-induced leukemo-lymphomogenicity in a transgenic mouse model. Leukemia *25*, 888-891.
Topp, M. S., Kufer, P., Gokbuget, N., Goebeler, M., Klinger, M., Neumann, S., Horst, H. A., Raff, T., Viardot, A., Schmid, M.*, et al.* (2011). Targeted therapy with the T-cell-engaging antibody blinatumomab of chemotherapy-refractory minimal residual disease in B-lineage acute lymphoblastic leukemia patients results in high response rate and prolonged leukemia-free survival. J Clin Oncol *29*, 2493-2498.
Trentin, L., Giordan, M., Dingermann, T., Basso, G., Te Kronnie, G., and Marschalek, R. (2009). Two independent gene signatures in pediatric t(4;11) acute lymphoblastic leukemia patients. Eur J Haematol *83*, 406-419.
Wang, Q. F., Wu, G., Mi, S., He, F., Wu, J., Dong, J., Luo, R. T., Mattison, R., Kaberlein, J. J., Prabhakar, S.*, et al.* (2011). MLL fusion proteins preferentially regulate a subset of wild-type MLL target genes in the leukemic genome. Blood *117*, 6895-6905.
Wei, J., Wunderlich, M., Fox, C., Alvarez, S., Cigudosa, J. C., Wilhelm, J. S., Zheng, Y., Cancelas, J. a., Gu, Y., Jansen, M.*, et al.* (2008). Microenvironment Determines Lineage Fate in a Human Model of MLL-AF9 Leukemia. Cancer Cell *13*, 483-495.
Wilkinson, A. C., Ballabio, E., Geng, H., North, P., Tapia, M., Kerry, J., Biswas, D., Roeder, R. G., Allis, C. D., Melnick, A.*, et al.* (2013). RUNX1 is a key target in t(4;11) leukemias that contributes to gene activation through an AF4-MLL complex interaction. Cell Rep *3*, 116-127.
Yokoyama, A., Lin, M., Naresh, A., Kitabayashi, I., and Cleary, M. L. (2010). A Higher-Order Complex Containing AF4 and ENL Family Proteins with P-TEFb Facilitates Oncogenic and Physiologic MLL-Dependent Transcription. Cancer Cell *17*, 198-212.

Figure Legends

Figure 1. Stably expressed MLL-Af4 in mouse HSPCs induces AML.

(A)Schematic of conserved domains contained within the MLL-AF4 and -Af4 fusion proteins.

(B) Western blot analysis showed MLL-Af4 expression in transduced Phoenix cells and MLL-AF4 expression in human t(4;11) cell lines (RS4;11 and SEM). Non-t(4;11) cell lines (U937 and REH) are negative control. anti-MLL antibody detects both wild type N-terminal MLL and fusion proteins.

(C) Comparison of retroviral titers of N-terminal MLL, MLL-AF4, and MLL-Af4. Result represents mean +- SD (n=3).

(D) Methylcellulose colony-forming assay of mouse HSPCs transduced with N-terminal MLL, MLL-AF4, and MLL-Af4. Results represents mean +- SD (n=3).

(E) Kaplan-Meier survival curves of mice transplanted with mouse HSPCs expressing MLL-AF4 or -Af4 using lymphoid (AF4 n=10; Af4 n=10) or myeloid conditions (AF4 n=10; Af4 n=10), and secondary transplantation of MLL-Af4 leukemic cells (n=5). Results were confirmed in independent experiments.

(F) Immunophenotype of MLL-Af4 leukemias by flow cytometry.

(G) Morphologic and immunohistochemical characterization of MLL-Af4 leukemias showed the immature myelomonocytic leukemic blast cells. Immunohistochemical staining of CD11b and B220 was done on spleen. Scale bar =10 um (PB and BM) and 50 um (spleen).

See also Figure S1 and Table S1.

Figure 2. Human CD34+ cells expressing MLL-Af4 initiate proB ALL in NSG mice.

(A) Flow cytometry analysis of BM and PB.

(B) Paraffin sections of spleen, liver and lung analyzed by hematoxylin and eosin staining (HE) or immunohistochemistry with human Ki67 showed infiltration of leukemic cells. Scale bar = 50 um.

(C) Wright-Giemsa-stained PB and BM cytospins showed the presence of malignant lymphoid blast cells. Scale bar = 10 um.

(D) Kaplan-Meier curve of leukemia-free recipient mice. One representative experiment is shown.

See also Figure S2 and Table S2.

Figure 3. MLL-Af4 proB ALL recapitulates t(4;11) disease at molecular level.

(A) Immunoprecipitation with FLAG antibody was performed in nuclear extracts of MLL-Af4 leukemic cells or control RS4;11 cells. The precipitates were immunoblotted with the antibodies against DOT1L, SEC components CDK9 and EAF2, or RPA70 as negative control.

(B) Growth curve of human CD34+ cells expressing MLL-Af4 in liquid culture upon treatment of DOT1L inhibitor EPZ-5676. Cells expressing leukemia oncogene MLL-AF9 and AML1-ETO were used as positive and negative controls for dependence on DOT1L activity, respectively.

(C) Heatmap showing the ChIP-seq signal of MLL-Af4 (FLAG), SEM MLL(N) & AF4(C) and RS4;11 MLL(N) & AF4(C) at all MLL-Af4 peaks, sorted by MLL-Af4 (FLAG) ChIP-seq signal. Arrow represents the centre of MLL-Af4 peaks. Window shows +/- 4kb from the peak centre. Scale bar represents log2 tags/bp/10^7.

(D) Example ChIP-seq tracks showing MLL-Af4 (FLAG), SEM MLL(N) & AF4(C) and RS4;11 MLL(N) & AF4(C) binding at *MEIS1* (top) and *RUNX1* (bottom).

(E) Fold-change ranked heatmap showed significantly differentially expressed MLL-AF4 activating (pink) and repressing (green) signature genes between MLL-Af4 leukemic cells and control proB cells. The signature genes were derived from Stam dataset by comparing MLL-AF4 patients to non-MLL rearranged ALL patients.

(F) GSEA showed that the MA4 activating/repressing signature derived from two published datasets was significantly enriched in MLL-Af4 and control proB cells, respectively.

See also Figure S3.

Figure 4. MLL-Af4 and MLL-AF9 lead to block at distinct B cell development stage.

(A) Flow cytometry analysis of MLL-Af4 and MLL-AF9 ALL.

(B) GSEA result of MLL-Af4 vs -AF9 showing proB gene signature was enriched in MLL-Af4, and preB gene signature was enriched in MLL-AF9 cells.

(C and D) Fold-change ranked heatmap showing significantly differentially expressed proB (pink) and preB (green) signature genes between homemade (C) and patient (D) MLL-Af4/AF4 and -AF9 ALL. Patient samples were from Andersson dataset.

See also Figure S4.

Figure 5. MLL-Af4 promotes distinct gene expression profiles via differential DNA binding.

(A and B) Principal component analysis (A) and unsupervised hierarchical clustering (B) of homemade MLL-Af4 and -AF9 leukemia together with MLL-fusion ALL patient samples based on the expression of a 100-gene discriminator from Andersson et al.

(C) Heatmap of *HOXA* gene expression of MLL-AF9, MLL-Af4 and control proB cells.

(D) Differential activation of reported MLL-fusion targets between MLL-AF9 and MLL-Af4 cells compared to proB cells. Expression data was derived from RNAseq, normalized by mean=0, variance=1.

(E) ChIP-qPCR analysis showed that MLL-Af4 and -AF9 have distinct chromatin occupancy at target gene loci correlating with gene expression in (D). *IVL* loci was used as negative control. The result represents mean and SD, n=2 biological replicates.

See also Figure S5 and S6.

Figure 6. MLL-Af4 maintains lymphoid potential after myeloid priming.

(A) CD33 and CD19 expression of MLL-Af4 and -AF9 cells in B-cell culture condition after initial priming in myeloid condition for 5 weeks.

(B) Flow cytometry of leukemia initiated by MLL-Af4 or -AF9 myeloid-primed cells in NSG mice.

(C) Flow cytometry analysis and Wright-Giemsa staining of CD33+CD19- sorted MLL-Af4 cells before and after lymphoid culture switch. Scale bar = 10 um.

(D) Heatmap showed increased expression of lymphoid genes and decreased expression of myeloid genes in CD33+CD19- cells expressing MLL-Af4 compared to those expressing MLL-AF9. All genes shown achieved a significance of $p \leq 0.05$ with fold change≥ 1.5.

See also Figure S7.

Figure 7. Phenotypic flexibility of t(4;11) ALL contributes to resistance to CD19-taregeted therapy.

(A) Schematic of lineage progression of the pediatric t(4;11) patient sample.

(B) Wright-Giemsa-staining of BM of pediatric t(4;11) patient with relapse AML. Scale bar=10 um.

(C) CD33/CD19 expression of leukemia cells from NSG mice reconstituted with the pediatric t(4;11) relapse AML sample.

(D) qPCR results of selected lineage genes in CD33+CD19- sorted cells for t(4;11) AML and cytogenetically normal AML. n=3 technical replicates, error bars represent SD.

(E) Immunophenotype comparison of the adult t(4;11) patient sample before and after blinatumomab treatment.

(F) Wright-Giemsa-staining of BM of the adult t(4;11) patient before and after blinatumomab treatment. Scale bar=10 um.

(G) Alpha-naphthyl-butyrate and CD33 staining of the adult t(4;11) patient sample relapsing from blinatumomab treatment. Scale bar= 50 um.

Figures

Figure 1

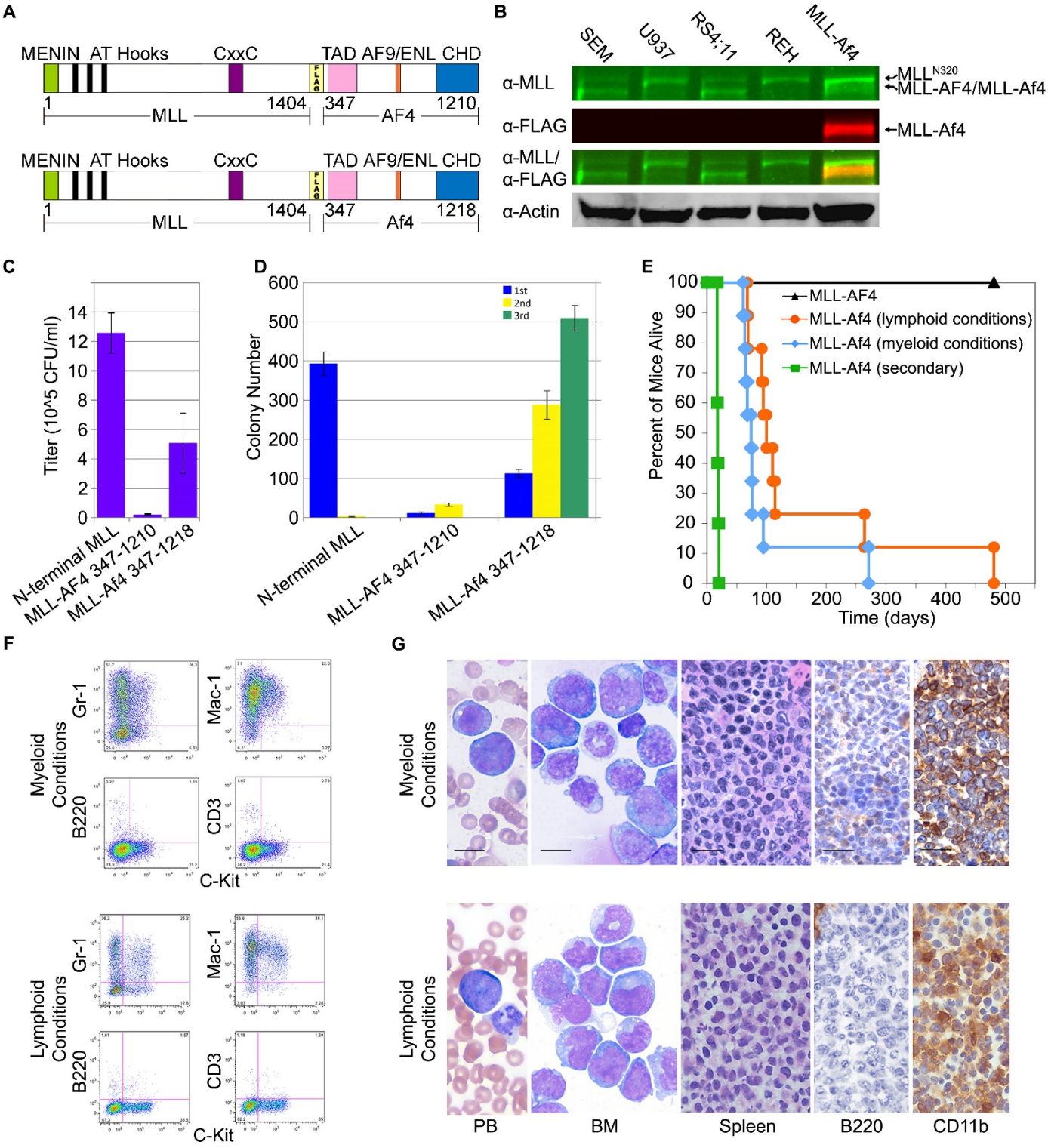

Figure 2

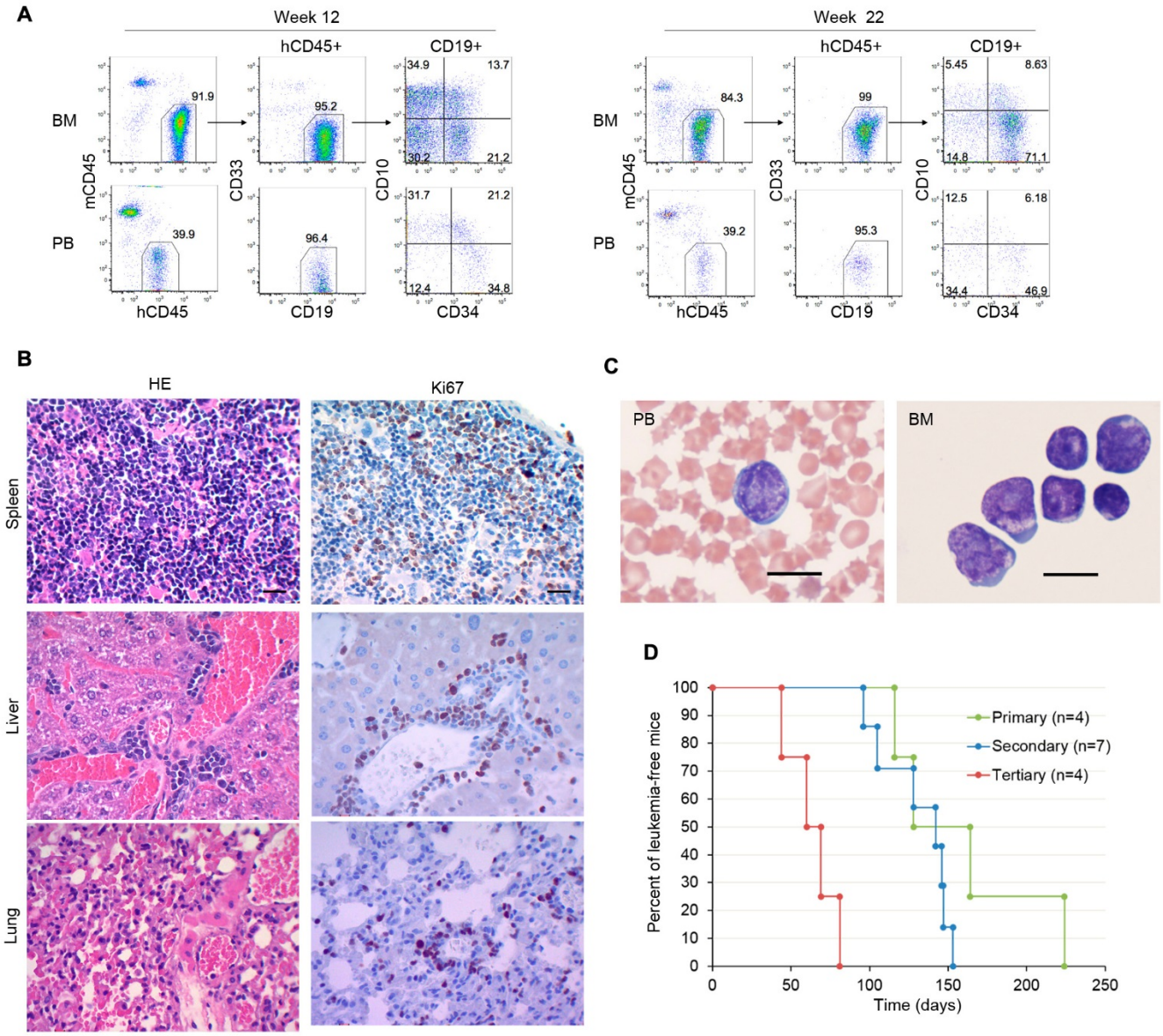
A
Week 12
hCD45+
CD19+
BM
PB
mCD45
hCD45
CD33
CD19
CD10
CD34
91.9
95.2
34.9
13.7
30.2
21.2
39.9
96.4
31.7
21.2
12.4
34.8
Week 22
84.3
99
5.45
8.63
14.8
71.1
39.2
95.3
12.5
6.18
34.4
46.9
B
HE
Ki67
Spleen
Liver
Lung
C
PB
BM
D
Percent of leukemia-free mice
Time (days)
Primary (n=4)
Secondary (n=7)
Tertiary (n=4)
0
10
20
30
40
50
60
70
80
90
100
0
50
100
150
200
250

Figure 3

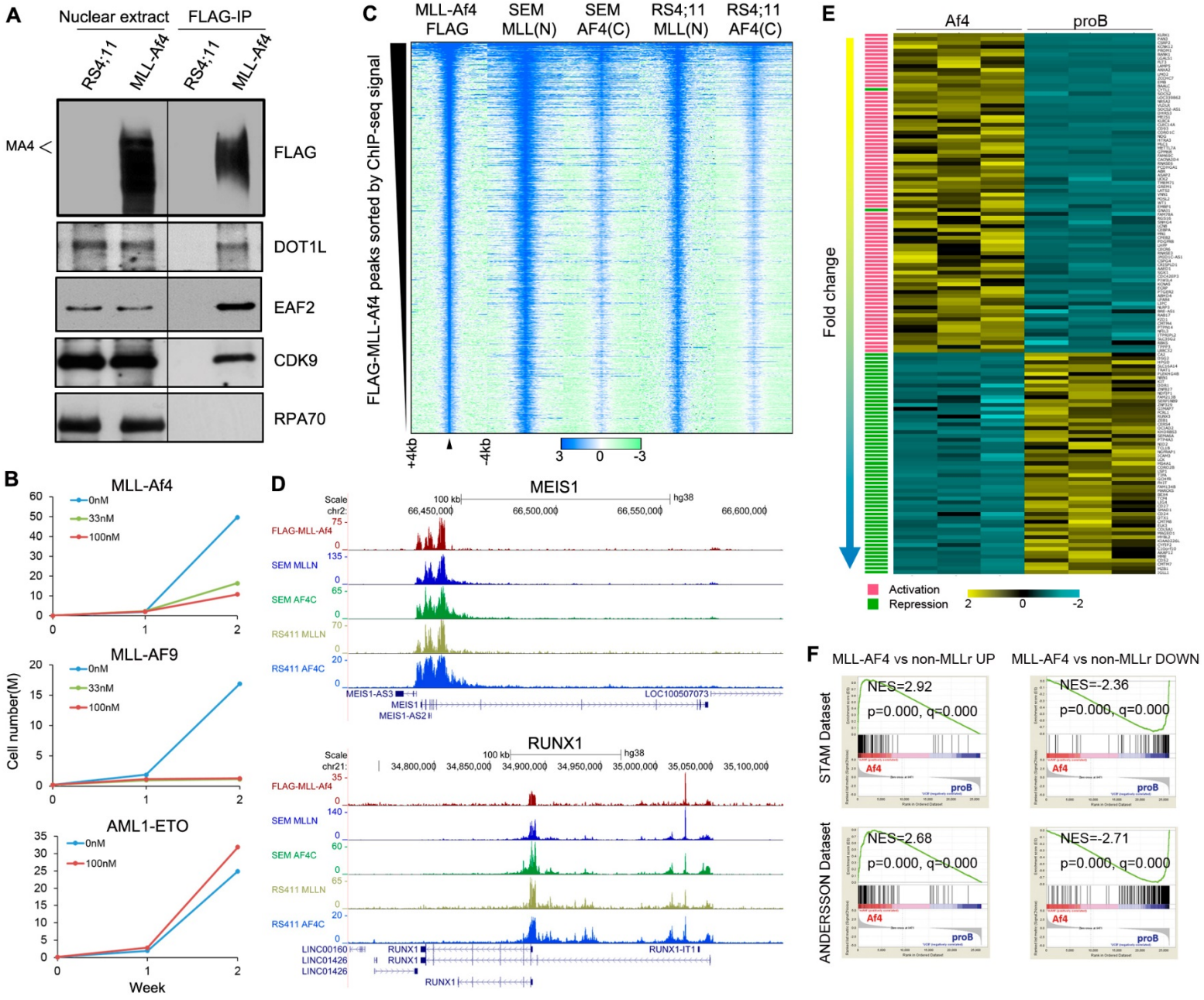
A
Nuclear extract
FLAG-IP
RS4;11
MLL-Af4
RS4;11
MLL-Af4
MA4 <
FLAG
DOT1L
EAF2
CDK9
RPA70
B
MLL-Af4
0nM
33nM
100nM
MLL-AF9
0nM
33nM
100nM
AML1-ETO
0nM
100nM
Cell number(M)
Week
C
MLL-Af4 FLAG
SEM MLL(N)
SEM AF4(C)
RS4;11 MLL(N)
RS4;11 AF4(C)
FLAG-MLL-Af4 peaks sorted by ChIP-seq signal
+4kb
-4kb
3
0
-3
D
MEIS1
Scale
chr2:
100 kb
hg38
66,450,000
66,500,000
66,550,000
66,600,000
FLAG-MLL-Af4
SEM MLLN
SEM AF4C
RS411 MLLN
RS411 AF4C
MEIS1-AS3
LOC100507073
MEIS1
MEIS1-AS2
RUNX1
Scale
chr21:
100 kb
hg38
34,800,000
34,850,000
34,900,000
34,950,000
35,000,000
35,050,000
35,100,000
FLAG-MLL-Af4
SEM MLLN
SEM AF4C
RS411 MLLN
RS411 AF4C
LINC00160
LINC01426
LINC01426
RUNX1
RUNX1
RUNX1-IT1
RUNX1
E
Af4
proB
Fold change
Activation
Repression
2
0
-2
F
MLL-AF4 vs non-MLLr UP
MLL-AF4 vs non-MLLr DOWN
STAM Dataset
NES=2.92
p=0.000, q=0.000
NES=-2.36
p=0.000, q=0.000
ANDERSSON Dataset
NES=2.68
p=0.000, q=0.000
NES=-2.71
p=0.000, q=0.000
Af4
proB

Figure 4

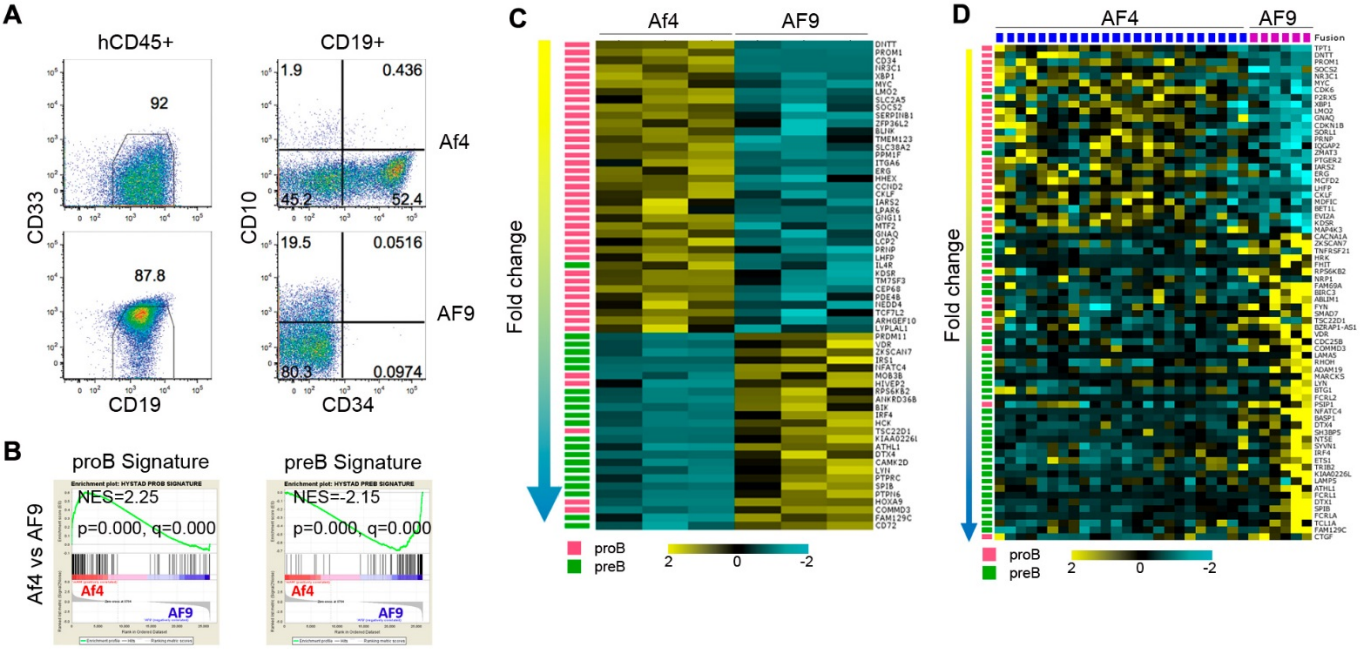
A
hCD45+
CD19+
92
87.8
CD33
CD19
1.9
0.436
45.2
52.4
Af4
19.5
0.0516
80.3
0.0974
AF9
CD10
CD34
B
proB Signature
preB Signature
NES=2.25
p=0.000, q=0.000
NES=-2.15
p=0.000, q=0.000
Af4 vs AF9
Af4
AF9
C
Af4
AF9
Fold change
proB
preB
2
0
-2
D
AF4
AF9
Fusion
Fold change
proB
preB
2
0
-2

Figure 5

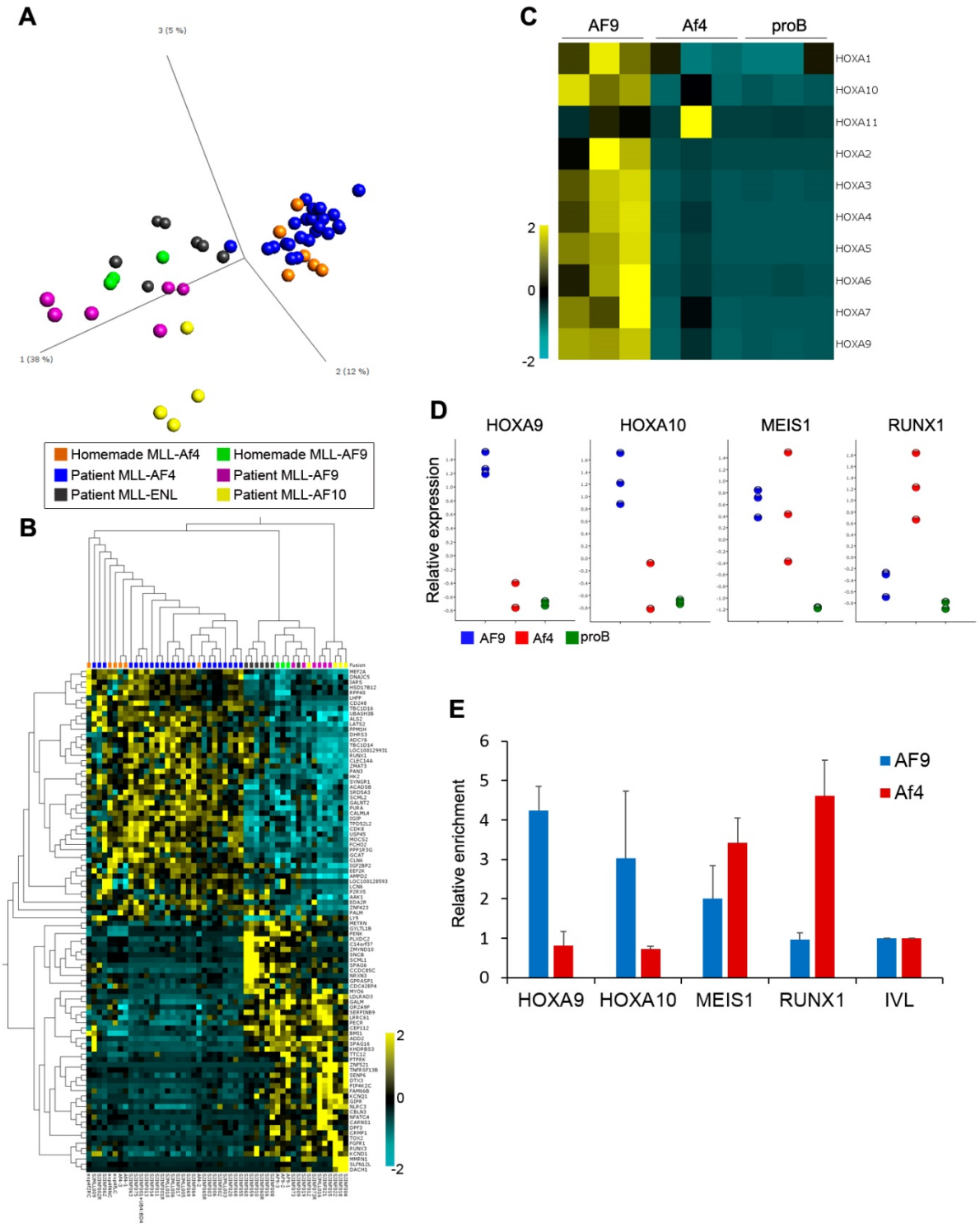
A
3 (5 %)
1 (38 %)
2 (12 %)
Homemade MLL-Af4
Homemade MLL-AF9
Patient MLL-AF4
Patient MLL-AF9
Patient MLL-ENL
Patient MLL-AF10
B
Fusion
2
0
-2
C
AF9
Af4
proB
HOXA1
HOXA10
HOXA11
HOXA2
HOXA3
HOXA4
HOXA5
HOXA6
HOXA7
HOXA9
2
0
-2
D
HOXA9
HOXA10
MEIS1
RUNX1
Relative expression
AF9
Af4
proB
E
Relative enrichment
6
5
4
3
2
1
0
AF9
Af4
HOXA9
HOXA10
MEIS1
RUNX1
IVL

Figure 6

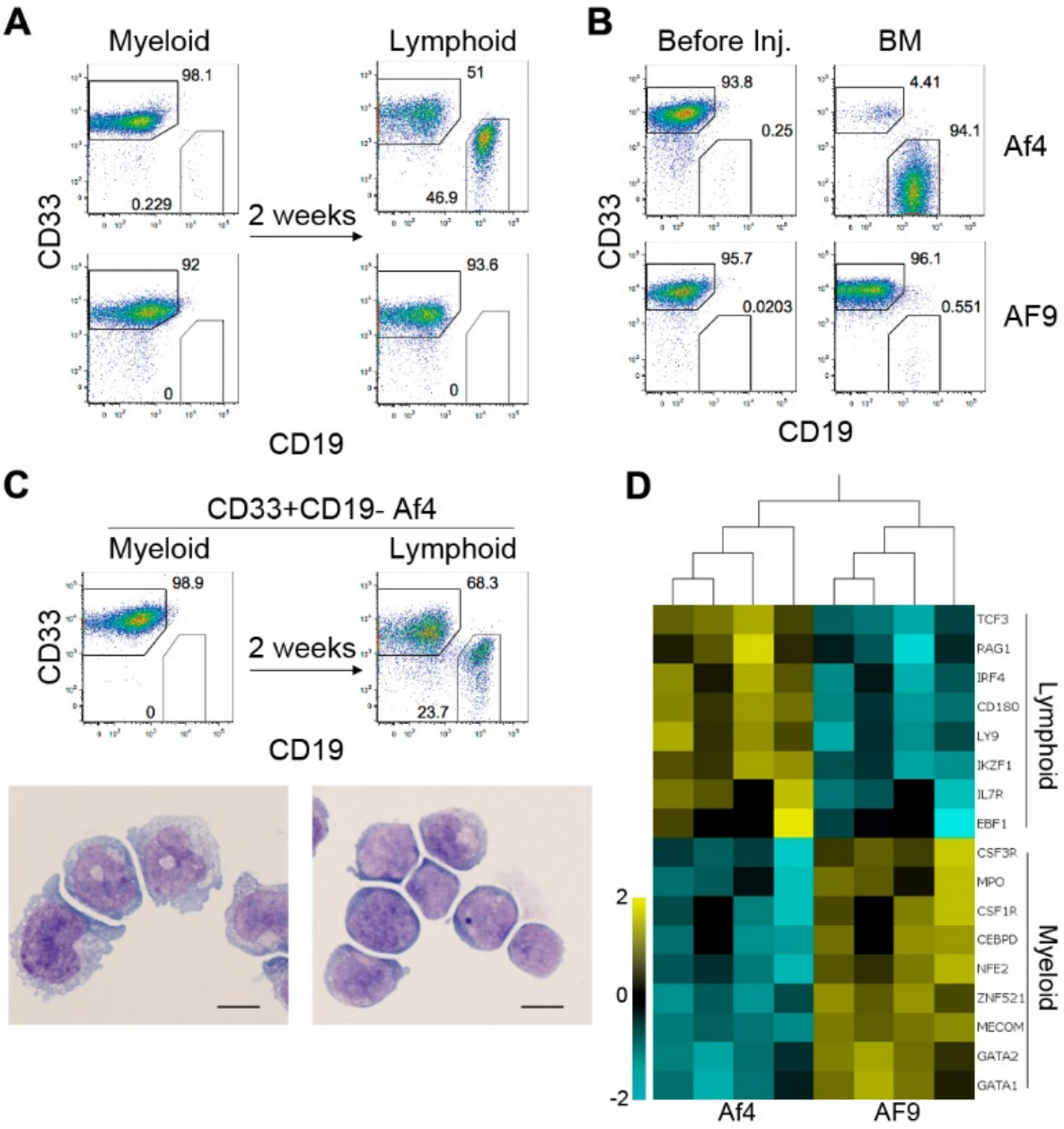
A
Myeloid
Lymphoid
98.1
0.229
51
46.9
92
0
93.6
0
2 weeks
CD33
CD19
B
Before Inj.
BM
93.8
0.25
4.41
94.1
95.7
0.0203
96.1
0.551
Af4
AF9
CD33
CD19
C
CD33+CD19- Af4
Myeloid
Lymphoid
98.9
0
68.3
23.7
2 weeks
CD33
CD19
D
TCF3
RAG1
IRF4
CD180
LY9
IKZF1
IL7R
EBF1
CSF3R
MPO
CSF1R
CEBPD
NFE2
ZNF521
MECOM
GATA2
GATA1
Lymphoid
Myeloid
2
0
-2
Af4
AF9

Figure 7

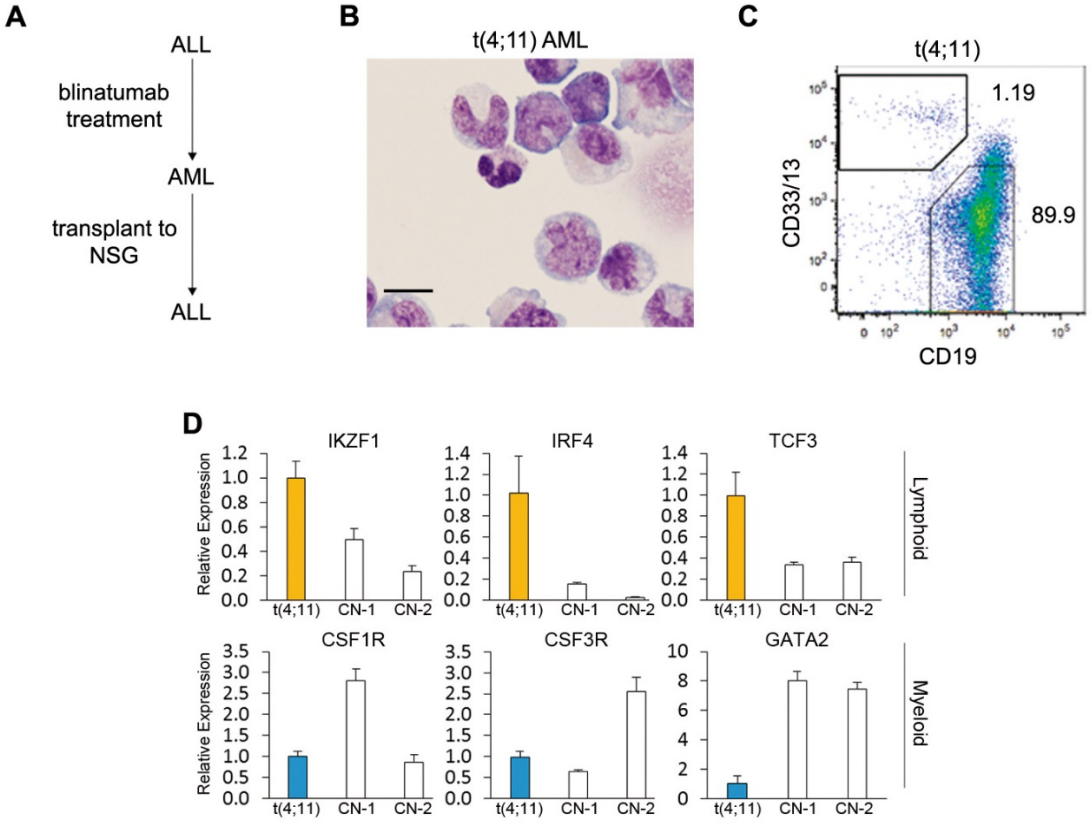

E

Prior to blinatumomab:	CD19+	TdT+	CD22+	CD79a+	CD14-	CD15+(partial)	CD33-
Relapse after blinatumomab:	CD19-	TdT-	CD22-	CD79a+ (partial)	CD14+	CD15+	CD33+

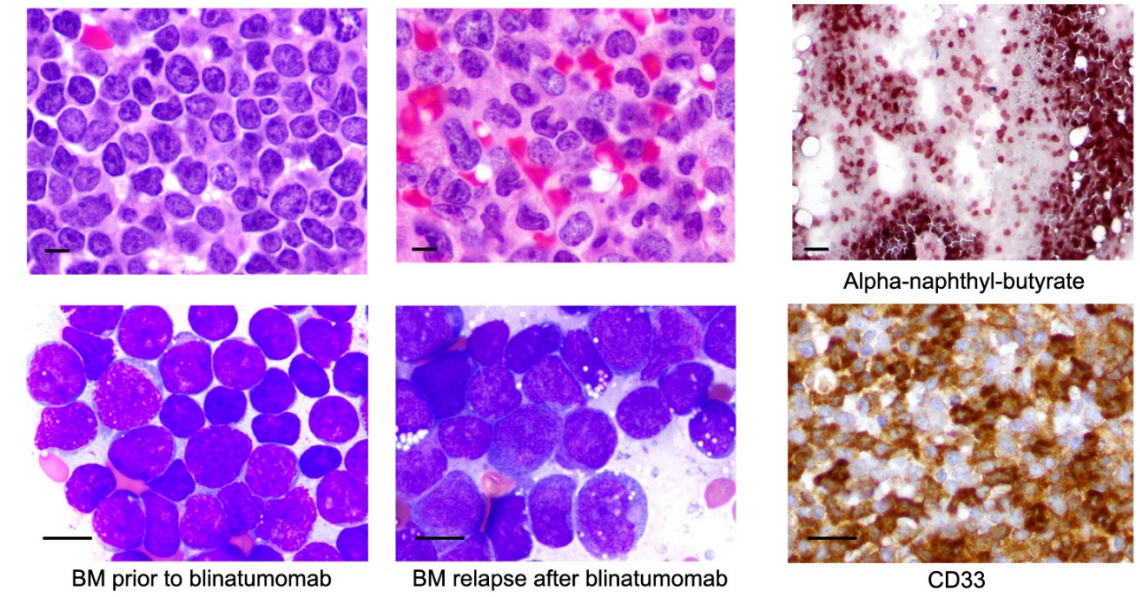

Supplemental Information

Figure S1

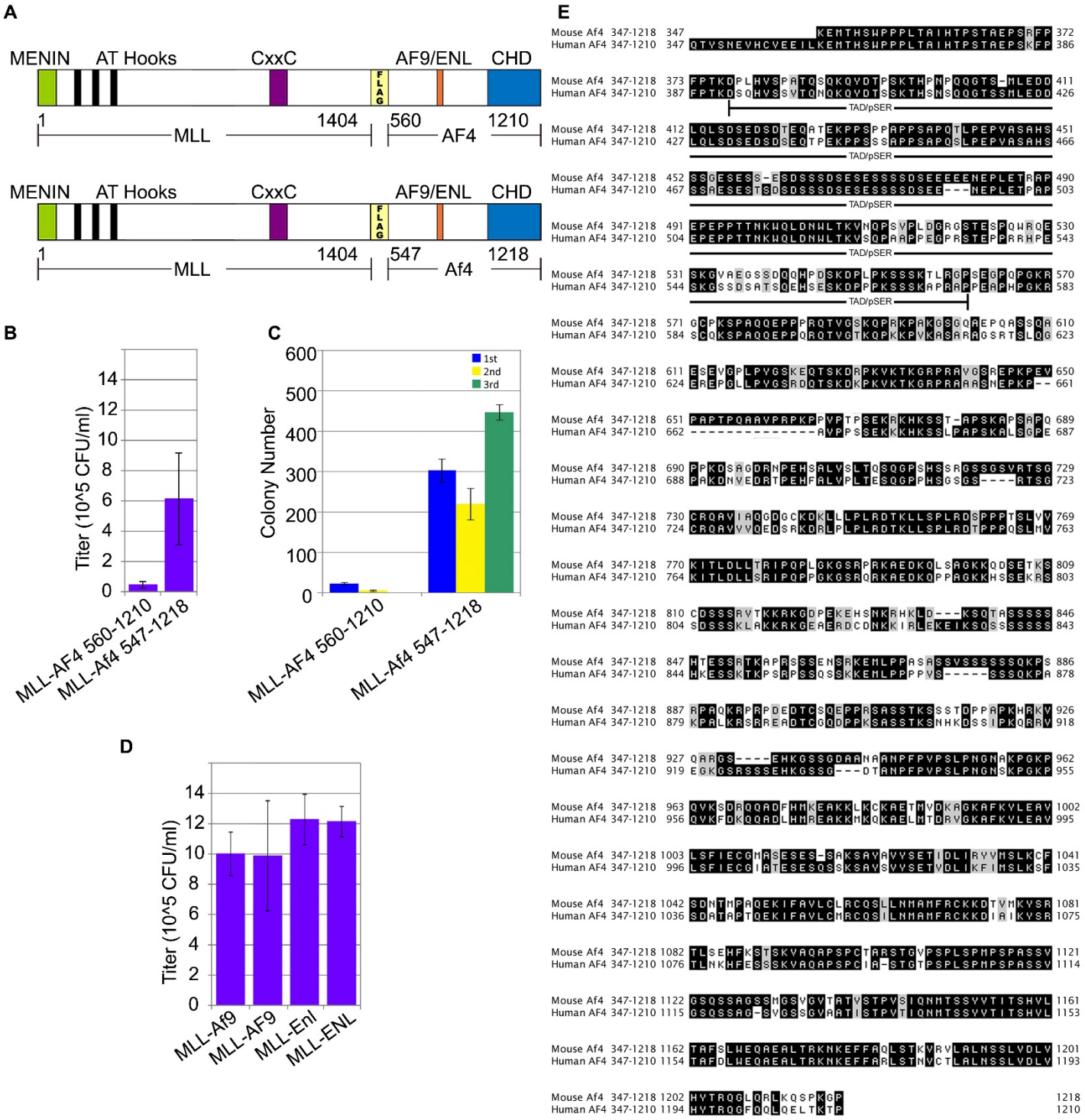

Figure S1, related to Figure 1. MLL-Af4 allows high retroviral titers.

(A) Schematic of conserved domains contained within the MLL-AF4 and -Af4 fusion proteins that truncate the Transcriptional Activation/Serine Rich domain of AF4 (TAD/pSER).

(B) Comparison of retroviral titers of MLL-AF4(560-1210) and MLL-Af4(547-1218). Results represent mean +- SD (n=3).

(C) Methylcellulose colony-forming assay of mouse HSPCs transduced MLL-AF4(560-1210) and MLL-Af4(547-1218). Results represent mean +- SE (n=3).

(D) Comparison of retroviral titers of MLL-Af9, MLL-AF9, MLL-Enl, and MLL-ENL. Results represent mean +- SD (n=3).

(E) Amino acid alignment of the mouse Af4 and human AF4 residues included in the MLL-Af4 and MLL-AF4 fusion constructs. Identical amino acid residues are indicated as black boxes and conservative changes are indicated as gray boxes. The bracket indicates the TAD/pSER domain.

Figure S2

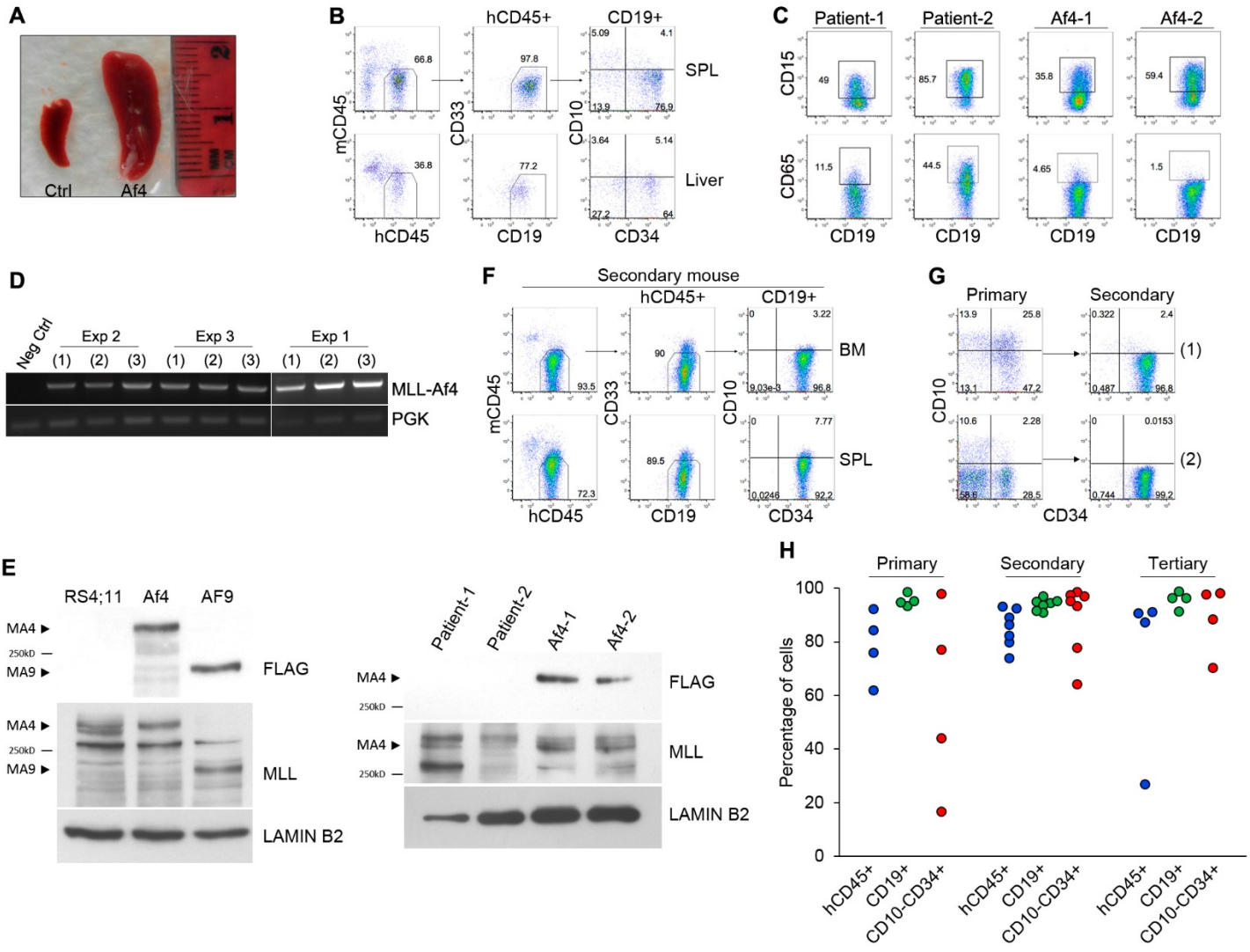
A
Ctrl
Af4
B
hCD45+
CD19+
mCD45
CD33
CD10
SPL
Liver
hCD45
CD19
CD34
C
Patient-1
Patient-2
Af4-1
Af4-2
CD15
CD65
CD19
D
Neg Ctrl
Exp 2
Exp 3
Exp 1
MLL-Af4
PGK
E
RS4;11
Af4
AF9
MA4
MA9
250kD
FLAG
MLL
LAMIN B2
Patient-1
Patient-2
Af4-1
Af4-2
F
Secondary mouse
BM
SPL
G
Primary
Secondary
(1)
(2)
H
Primary
Secondary
Tertiary
Percentage of cells
hCD45+
CD19+
CD10-CD34+

Figure S2, related to Figure 2. Characterizing MLL-Af4 leukemic mice.

(A) Splenomegaly was consistently found in NSG mice reconstituted with MLL-Af4 cells.

(B) Flow cytometry analysis of spleen and liver confirmed the infiltration of the leukemic cells with proB-ALL phenotype.

(C)Flow cytometry analysis of CD15 and CD65 expression on CD19+ MLL-Af4 leukemic cells and t(4;11) patient xenografts. Two representative experiments are shown.

(D) Results of RT-PCR confirmed the expression of MLL-Af4 in leukemic cells. 9 individual mice from 3 independent experiments are shown. Human cells without transduction were used as negative control.

(E) Immunoblot analysis showed the expression of MLL-Af4 protein in leukemic cells was comparable to MLL-AF4 expression in t(4;11) cell line (RS4;11) and patient samples. Human cells expressing MLL-AF9 were used as control.

(F) Flow cytometry analysis showed the disease of secondary leukemic mice had the same proB-ALL phenotype.

(G) Compared to disease of primary mice, the CD34+CD10- compartment increased in secondary disease. Two representative experiments are shown.

(H) Summary of cell surface marker expression in leukemic mice shown in (G).

Figure S3

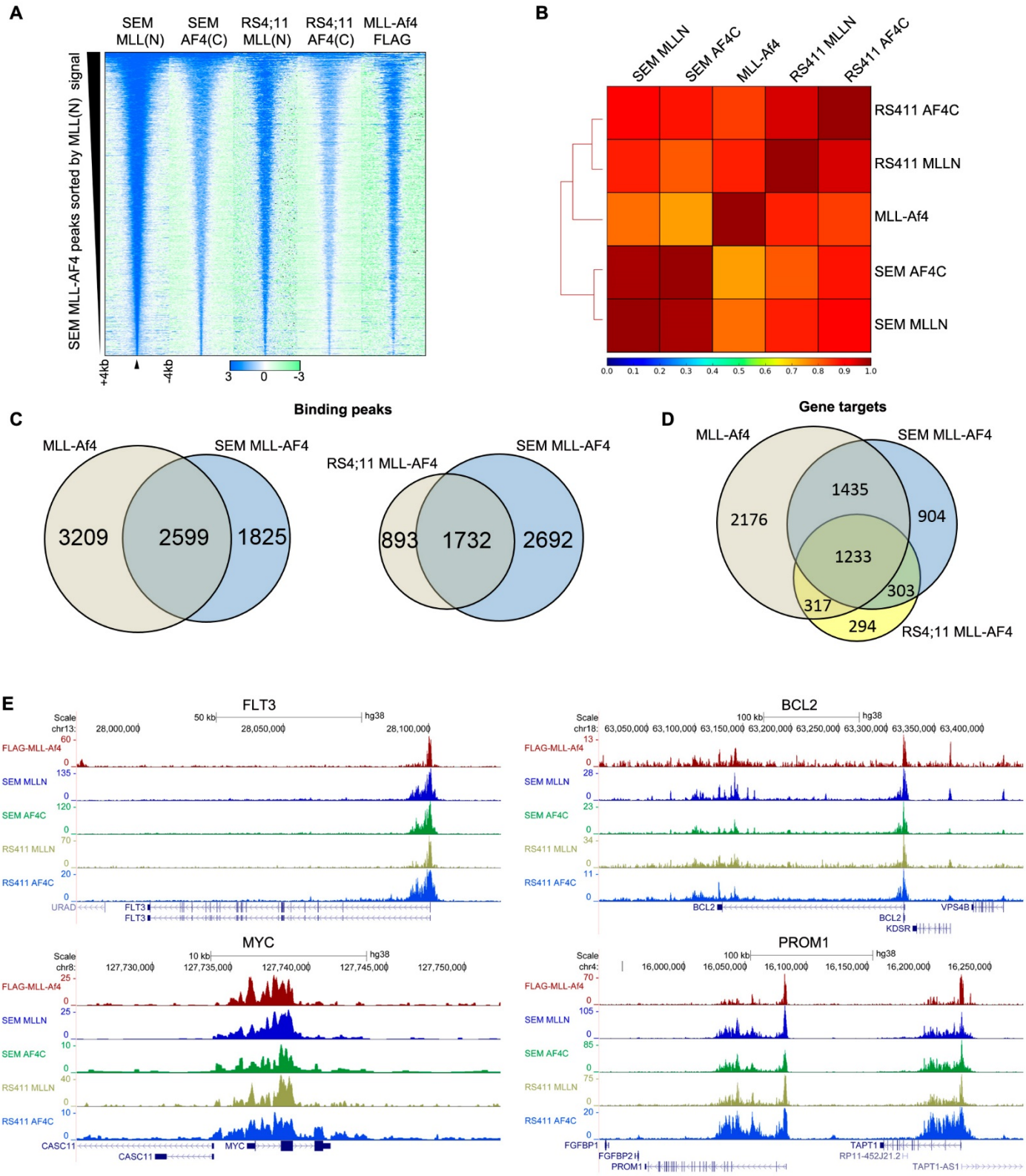
A
SEM MLL(N)
SEM AF4(C)
RS4;11 MLL(N)
RS4;11 AF4(C)
MLL-Af4 FLAG
SEM MLL-AF4 peaks sorted by MLL(N) signal
+4kb
-4kb
3 0 -3
B
SEM MLLN
SEM AF4C
MLL-Af4
RS411 MLLN
RS411 AF4C
RS411 AF4C
RS411 MLLN
MLL-Af4
SEM AF4C
SEM MLLN
0.0 0.1 0.2 0.3 0.4 0.5 0.6 0.7 0.8 0.9 1.0
C
Binding peaks
MLL-Af4
SEM MLL-AF4
3209
2599
1825
RS4;11 MLL-AF4
SEM MLL-AF4
893
1732
2692
D
Gene targets
MLL-Af4
SEM MLL-AF4
RS4;11 MLL-AF4
2176
1435
904
1233
303
317
294
E
FLT3
Scale
chr13:
28,000,000
28,050,000
28,100,000
50 kb
hg38
FLAG-MLL-Af4
SEM MLLN
SEM AF4C
RS411 MLLN
RS411 AF4C
URAD
FLT3
FLT3
BCL2
Scale
chr18:
63,050,000
63,100,000
63,150,000
63,200,000
63,250,000
63,300,000
63,350,000
63,400,000
100 kb
hg38
FLAG-MLL-Af4
SEM MLLN
SEM AF4C
RS411 MLLN
RS411 AF4C
BCL2
VPS4B
BCL2
KDSR
MYC
Scale
chr8:
127,730,000
127,735,000
127,740,000
127,745,000
127,750,000
10 kb
hg38
FLAG-MLL-Af4
SEM MLLN
SEM AF4C
RS411 MLLN
RS411 AF4C
CASC11
MYC
CASC11
PROM1
Scale
chr4:
16,000,000
16,050,000
16,100,000
16,150,000
16,200,000
16,250,000
100 kb
hg38
FLAG-MLL-Af4
SEM MLLN
SEM AF4C
RS411 MLLN
RS411 AF4C
FGFBP1
FGFBP2
PROM1
TAPT1
RP11-452J21.2
TAPT1-AS1

Figure S3, related to Figure 3. MLL-Af4 occupies the corresponding genome regions as MLL-AF4.

(A) Heat-map showing the ChIP-seq signal of SEM MLL(N) & AF4(C), RS4;11 MLL(N) & AF4(C) and MLL-Af4 (FLAG) at all SEM MLL-AF4 peaks, sorted by SEM MLL(N) ChIP-seq signal. Arrow represents the centre of SEM MLL-AF4 peaks. Window shows +/- 4kb from the peak centre. Scale bar represents log2 tags/bp/10^7.

(B) Heat-map representing Pearson correlation between read coverage of SEM MLL(N) & AF4(C), MLL-Af4 (FLAG) and RS411 MLL(N) & AF4(C), at all SEM MLL-AF4 peaks. Scale bar represents the correlation coefficient.

(C) Venn diagrams showing the overlap of MLL-Af4 peaks with SEM MLL-AF4 peaks (top) and SEM MLL-AF4 peaks with RS4;11 MLL-AF4 peaks (bottom). Overlap was defined as an exact intersection between peaks with no gap allowed.

(D) Venn diagram showing the overlap of gene targets bound by MLL-Af4, SEM MLL-AF4 or RS4;11 MLL-AF4 at the promoter (TSS +/- 2kb)

(E) Example ChIP-seq track showing MLL-Af4 (FLAG), SEM MLL(N) & AF4(C) and RS4;11 MLL(N) & AF4(C) ChIP-seq at FLT3, BCL2, MYC and PROM1.

Figure S4

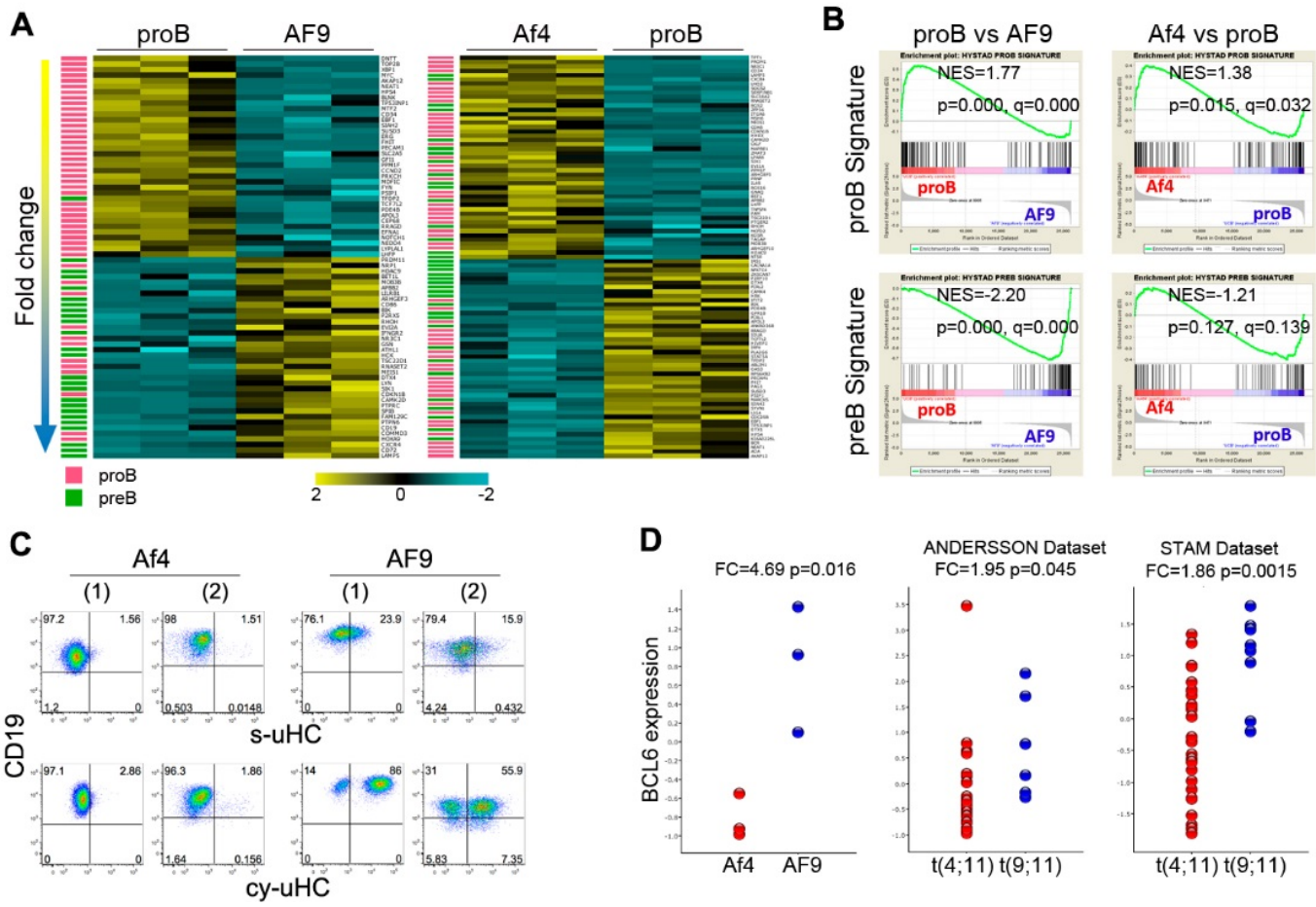
A
proB
AF9
Af4
proB
Fold change
proB
preB
2
0
-2
B
proB vs AF9
Af4 vs proB
proB Signature
preB Signature
NES=1.77
p=0.000, q=0.000
NES=1.38
p=0.015, q=0.032
NES=-2.20
p=0.000, q=0.000
NES=-1.21
p=0.127, q=0.139
C
Af4
AF9
(1)
(2)
CD19
s-uHC
cy-uHC
97.2
1.56
1.2
0
98
1.51
0.503
0.0148
76.1
23.9
0
0
79.4
15.9
4.24
0.432
97.1
2.86
0
0
96.3
1.86
1.64
0.156
14
86
0
0
31
55.9
5.83
7.35
D
FC=4.69 p=0.016
ANDERSSON Dataset
FC=1.95 p=0.045
STAM Dataset
FC=1.86 p=0.0015
BCL6 expression
Af4
AF9
t(4;11)
t(9;11)
t(4;11)
t(9;11)

Figure S4, related to Figure 4. MLL-Af4 and MLL-AF9 B ALL cells are blocked at different developmental stages.

(A) Fold-change ranked heatmaps showed significantly differentially expressed proB (pink) and preB (green) signature genes in proB vs MLL-AF9, and MLL-Af4 vs proB comparisons.

(B) GSEA result of proB vs MLL-AF9 comparisons show proB gene signature was enriched in control proB cells, and preB gene signature was enriched in MLL-AF9 cells. Less significant enrichment was achieved in MLL-Af4 vs proB comparison.

(C) Flow cytometry staining for surface (s) and cytoplasmic (cy) uHC of MLL-Af4 and -AF9 ALL. Two independent experiments are shown.

(D) RNAseq or microarray analysis comparing BCL6 expression of MLL-AF9 cells versus MLL-Af4/AF4 cells in model system and patient samples in Andersson dataset (t(4;11) n=24, t(9;11) n=6) and Stam dataset (t(4;11) n=29, t(9;11) n=8, Probeset=203140_at). The p values were calculated by two-tailed t-test.

Figure S5

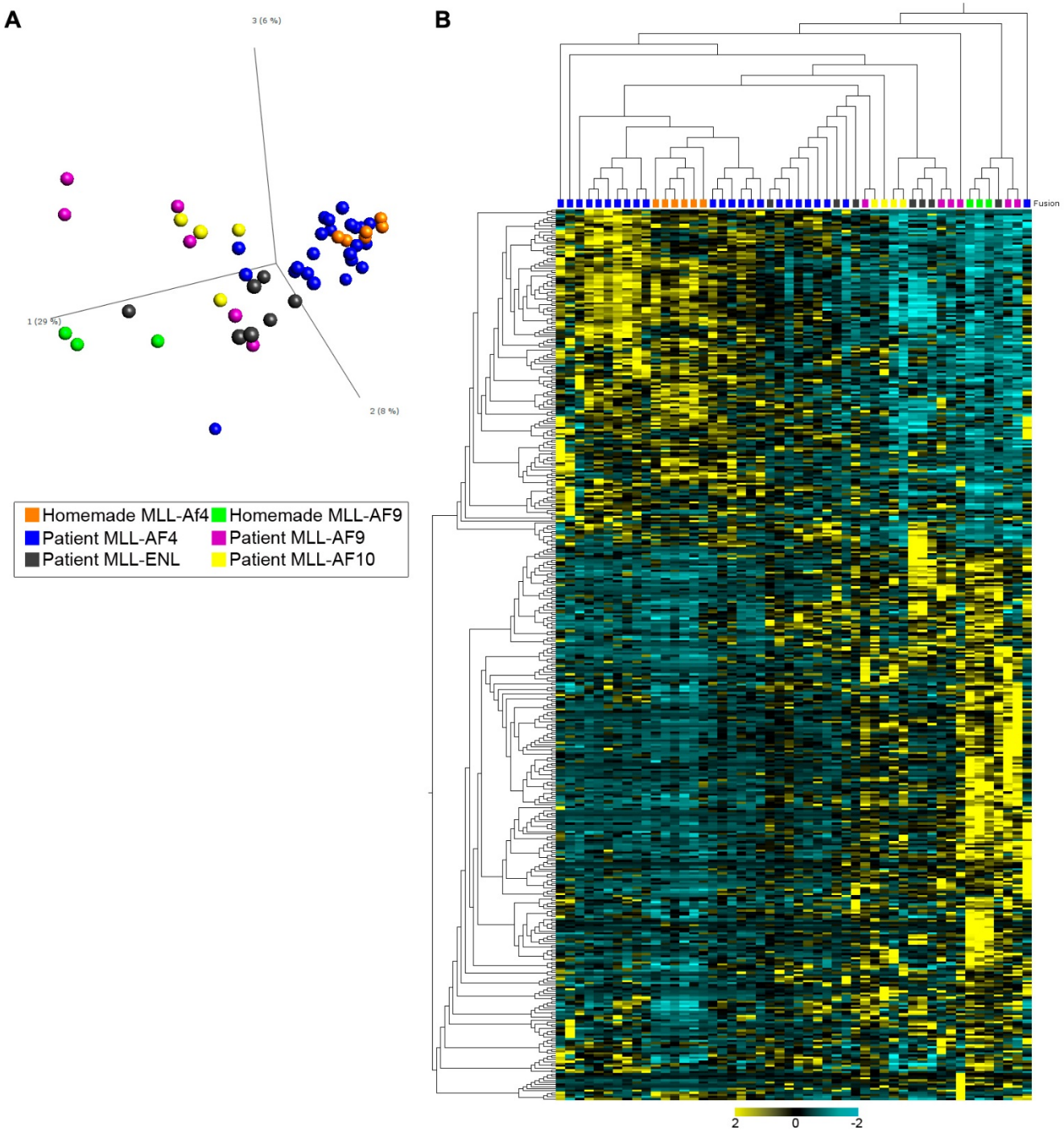
A
3 (6 %)
1 (29 %)
2 (8 %)
Homemade MLL-Af4
Homemade MLL-AF9
Patient MLL-AF4
Patient MLL-AF9
Patient MLL-ENL
Patient MLL-AF10
B
Fusion
2
0
-2

Figure S5, related to Figure 5. MLL-Af4 gene expression profile recapitulates t(4;11) specific molecular signature.

(A and B) PCA (A) and unsupervised hierarchical clustering (B) of homemade MLL-Af4 and -AF9 leukemia together with MLL-fusion ALL patient samples in Andersson dataset showed MLL-Af4 leukemia clustered tightly with MA4 patient samples. The analysis was based on the expression of 430 genes which were most significantly differential expressed between homemade MLL-Af4 and -AF9 leukemic cells (Table S7).

Figure S6

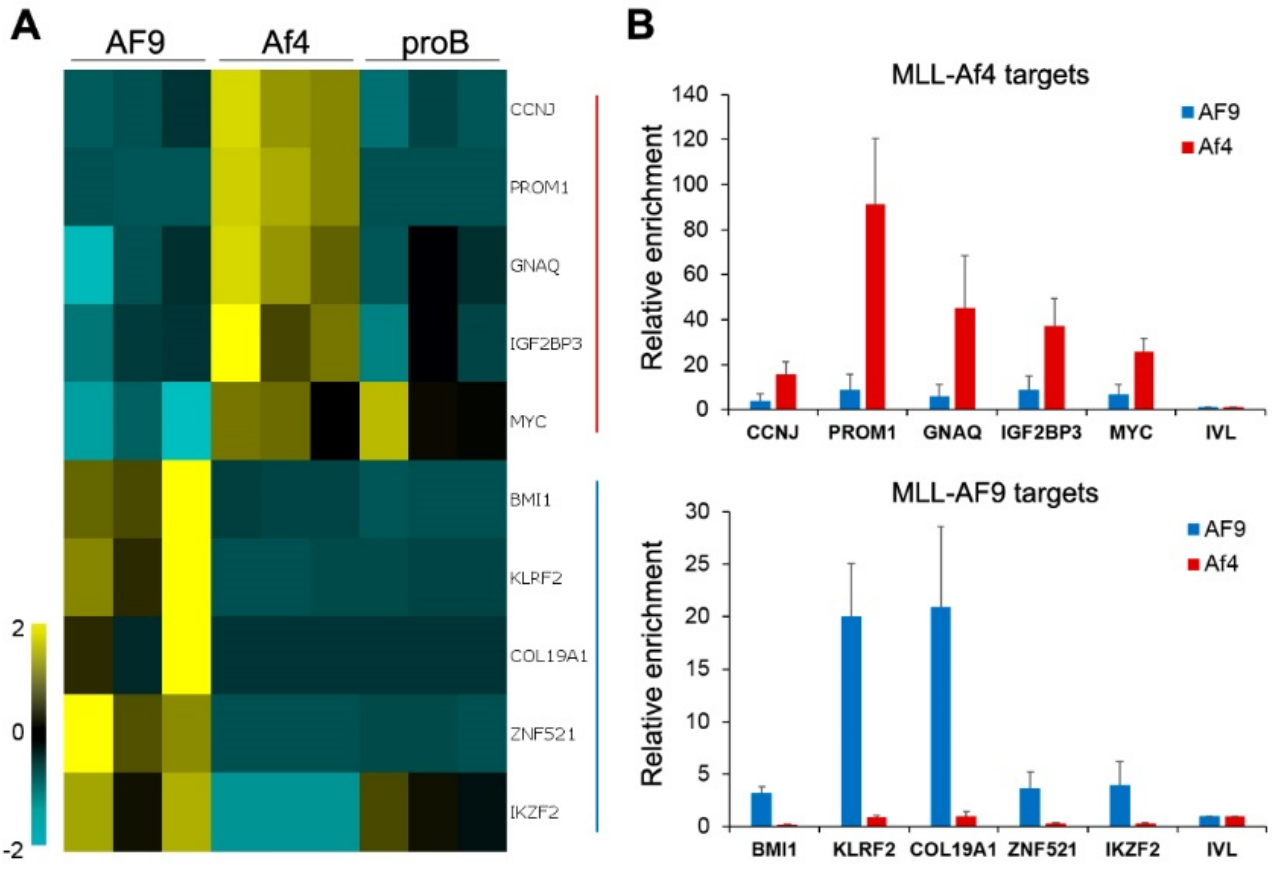
A
AF9
Af4
proB
CCNJ
PROM1
GNAQ
IGF2BP3
MYC
BMI1
KLRF2
COL19A1
ZNF521
IKZF2
2
0
-2
B
MLL-Af4 targets
Relative enrichment
AF9
Af4
CCNJ
PROM1
GNAQ
IGF2BP3
MYC
IVL
MLL-AF9 targets
BMI1
KLRF2
COL19A1
ZNF521
IKZF2

Figure S6, related to Figure 5. Differential gene expression associated with differential DNA binding between MLL-Af4 and -AF9.

(A) Heatmap of selected genes specifically expressed in MLL-Af4 or -AF9 ALL and comparison with control proB cell expression.

(B) ChIP-qPCR analysis showed that MLL-Af4 and -AF9 have corresponding chromatin occupancy at their specific target gene loci. IVL loci was used as negative control. The result represents mean and SD, n=3 biological replicates.

Figure S7

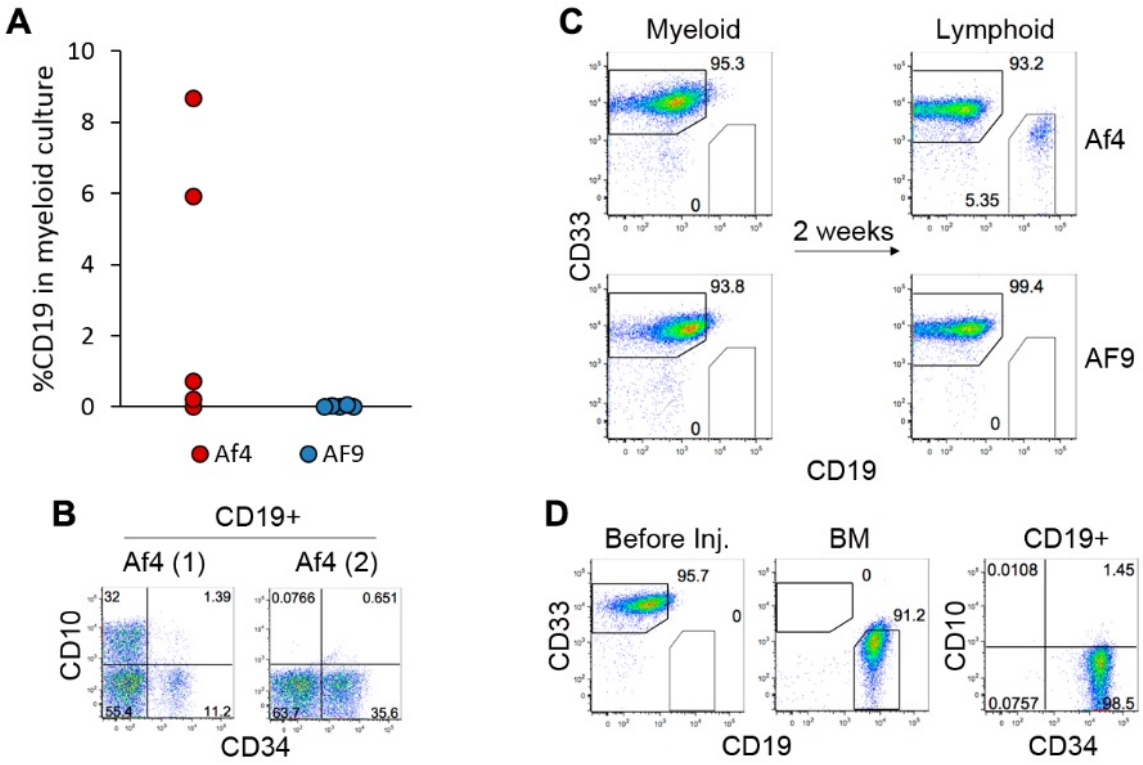

E

STANDARD_NAME	pValue	FDR	
GSE10325_LUPUS_BCELL_VS_LUPUS_MYELOID_UP	1.41E-06	7.73E-05	Af4 Up
GSE10325_BCELL_VS_MYELOID_UP	0.000353	0.005629	AF9 Down
GSE10325_BCELL_VS_MYELOID_DN	3.96E-13	4.09E-11	
GSE10325_LUPUS_BCELL_VS_LUPUS_MYELOID_DN	2.7E-08	1.06E-06	Af4 Down
GSE22886_NAIVE_BCELL_VS_NEUTROPHIL_DN	1.25E-06	3.38E-05	AF9 Up
GSE29618_BCELL_VS_MONOCYTE_DN	6.48E-05	0.001062	

Figure S7, related to Figure 6. MLL-Af4 cells keep an active lymphoid program under myeloid condition.

(A)Percentage of CD33-CD19+ cells in MLL-Af4 and -AF9 cultures primed in myeloid conditions for 5 weeks. Five independent experiments are shown.

(B) Leukemia initiated by myeloid-primed MLL-Af4 cells had proB immunophenotype. Two independent experiments are shown.

(C and D) A particular MLL-Af4 myeloid culture without detectable CD33-CD19+ cells gave rise to CD19+ B cells both in-vitro (C) and in NSG mice (D).

(E) Dataset enrichment analysis by L-Path showed B cell signature is associated with CD33+CD19- cells expressing MLL-Af4 cells compared to those expressing MLL-AF9. Datasets enriched in genes upregulated or downregulated by MLL-Af4 were colored red and green, respectively.

Table S1. Hemogram of representative leukemic C57BL/6 mice.

Myeloid Conditions

	Spleen g	WBC $x10^3$	RBC $x10^6$	Hgb g/dL	Hct %	Plt $x10^3$
1	0.58	20	4.4	9.2	28	368
2	0.70	28	4.9	8.4	25	416
3	0.32	4	5.6	10.0	30	112
4	0.88	44	5.8	8.4	29	250
5	0.58	15	4.5	8.8	28	384
6	0.76	26	4.1	9.8	29	187
Avg	0.64	23	4.9	9.1	28	286
±SD	0.19	13	0.7	0.7	2	122

Lymphoid Conditions

	Spleen g	WBC $x10^3$	RBC $x10^6$	Hgb g/dL	Hct %	Plt $x10^3$
1	0.95	85	4.0	8.4	25	636
2	0.24	9	5.7	7.8	25	494
3	0.70	21	4.1	9.4	28	384
4	0.79	68	6.1	9.2	28	300
5	0.61	11	4.6	8.7	28	468
6	1.05	49	5.9	9.2	32	372
Avg	0.72	41	5.1	8.8	28	442
±SD	0.29	32	0.9	0.6	3	118

Secondary Transplant

	Spleen g	WBC $x10^3$	RBC $x10^6$	Hgb g/dL	Hct %	Plt $x10^3$
1	0.67	36	4.4	10.8	30	240
2	0.64	40	3.6	8.6	27	210
3	0.77	10	4.4	8.9	26	268
Avg	0.69	28	4.1	9.4	28	239
±SD	0.07	16	0.4	1.2	2	29

Table S2. Summary of MLL-Af4 xenograft experiments.

Experiment No.	1	2	3	4
CD34+ source	CB	PBPC	CB	CB
Primary mice (#ALL/#Total)	4/4	3/3	3/3	3/3
# of primary mice used for secondary transplantation	2	2	3	-
Secondary mice (#ALL/#Total)	7/7	5/5	7/7	-
# of secondary mice used for tertiary transplantation	2	2	-	-
Tertiary mice (#ALL/#Total)	4/4	5/5	-	-

Table S3. QPCR primers.

Table S4. MLL-AF4 ALL signature from patient dataset.

Table S5. proB and preB signature.

Table S6. Andersson 100-gene.

Table S7. Differential signature genes between homemade ALL of MLL-Af4 and MLL-AF9.

Supplemental Experimental Procedures

Myeloid culture and B cell assay

To prime cells into myeloid lineage, MLL-Af4 and -AF9 transduced cells were cultured in IMDM with 10% fetal bovine serum (FBS) and supplemented with SCF, IL-3, IL-6, FLT3L, and TPO (10ng/mL). For B cell assay, myeloid-primed cells were transferred on to MS-5 stroma cells, maintained in aMEM with 10% FBS and supplemented with SCF, FLT3L, and IL-7 (10ng/mL). Half of the media/cells were removed and replaced with fresh media weekly.

Flow cytometry and Cell Sorting

Cells from mouse tissues were incubated with nonspecific binding blocker (anti-mouse/human CD16/CD32 Fc g receptor; BD) before staining. Antibodies (all BD unless noted) used were PE-CD10 (HI10a), APC- and PE-CD33 (WM53), PECy5-CD34 (581), V450-human CD45 (HI30), APCCy7-mouse CD45 (30-F11), PE-CD13 (WM15), PECy7-CD19 (5J25C1), PE-CD65(VIM8), FITC-CD15 (MMA), VioBlue-CD19 (6D5, Miltenyi), FITC-and BV421- uHC (H15101 Caltag Laboratories; MHM88, Biolegend), FITC- c-Kit and PE-CD11b, Gr-1, CD3, or B220 antibodies (eBioscience). Intracellular staining was performed using Cytofix/Cytoperm kit (BD). Cells were analyzed on FACSCanto flow cytometer (BD) or sorted on FACSAria (BD) or MoFlo XDP (Beckman Coulter), and the data was analyzed with FloJo software (TreeStar).

Methylcellulose colony-forming assays

Infection of lineage-depleted (Lin-) BM cells obtained from C57BL6 mice five days after 5-fluorouracil treatment and culture of the transduced progenitor cells in methylcellulose were performed as previously described (Luo et al, 2001). 30,000 cells were used for each transduction. The BM progenitor cells were centrifuged in retroviral supernatant at 2500g for 4 hours at 33^{o}C (spinoculation). The cells were incubated in fresh media with appropriate growth factors for 20 hours and spinoculation was repeated. Transformation capability of MLL-fusion constructs were examined in duplicate in at least 2 independent methylcellulose colony-forming assays.

Mouse bone marrow transduction and transplantation

The BM progenitor cells were centrifuged in retroviral supernatant at 2500g for 4 hours at 33^{o}C. For each mouse, 30,000 Lin- cells were spinoculated separately, and the transduced cells were

not pooled prior to transplant. The cells were incubated in fresh media with appropriate growth factors for 20 hours and spinoculation was repeated. Each mouse was transplanted by intravenous injection with transduced Lin- BM cells. For histological analysis, tissues were fixed in formalin, sectioned, and stained with hematoxylin and eosin. For immunohistochemical analysis, tissues were snap frozen in Tissue-Tek O.C.T. compound (Sikura), sectioned, and stained with antibodies to CD11b and B220. All experiments were performed in accordance with U of Chicago institutional guidelines.

Xenograft transplantation of cultured cells and patient samples

For cell line experiments, MLL-Af4 or -AF9 cells were primed in myeloid conditions for 4-8 weeks, and then 0.5-1M cells were injected through tail vein. For patient sample study, 1M t(4;11) AML cells were injected through tail vein. Each experiment was performed at least in three independent replicates. All experiments were performed in accordance with CCHMC institutional guidelines.

Western blotting

Nuclear lysates were obtained using NE-PER nuclear extraction kit (Thermo Scientific). Protein samples were run on 6% or 4-15% polyacrylamide gels and transferred overnight at 4°C to a nitrocellulose membrane. The primary antibodies used were anti-Flag (Cell Signalling Technology #2368 and Sigma M2), anti-Lamin B2 (Cell Signalling Technology #12255), anti-MLL (Bethyl A300-086A) and anti-Actin (NeoMarker ACTN05). The secondary antibodies were HRP-linked goat anti-rabbit IgG and anti-mouse IgG at 1:1000 (Cell Signaling Technology #7074, #7076), the signal of which was developed through ECL reaction; or goat anti-rabbit

IRDye 800RD and goat anti-mouse IRDye 680RD (Odyssey) at 1:10000, where the signal was visualized by fluorescent illumination (Odyssey CLx).

Immunoprecipitation

The crude nuclear pellet was lysed in 300-lysis buffer (40 mM Hepes pH 7.9, 300 mM NaCl, 1 mM EDTA, 1% Triton, 0.1% IGEPAL, 0.5 mM sodium orthovanadate, 50 mM sodium fluoride, protease inhibitor cocktail). The lysate was centrifuged at high speed. The clarified lysate was processed directly as described below or incubated with ethidium bromide (100 µg/mL) to check whether the interaction is mediated via DNA. For the purification of protein with FLAG tag, the clarified lysate was incubated in 1.5 mL tubes with 25 µL anti-FLAG M2 agarose (Sigma) beads overnight, washed four times with 300-lysis buffer with 15 min rotation at 4°C, and eluted with 3XFLAG peptide (Sigma) for 1 h on ice. The bound protein complex was resolved on an 8%–16% SDS-PAGE gel and were immunoblotted with following antibodies: anti- RPA70 (Cell Signaling Technology #2267), anti-CDK9 (Cell Signaling Technology #2316), anti-DOT1L (Bethyl A300-953A) and anti-EAF2 (Simone et al., 2003).

Chromatin immunoprecipitation (ChIP)

Dynabeads protein G (Invitrogen) pre–incubated with BSA and antibody against Flag (Sigma, M2) were used for IP. The immunoprecipitated DNA was purified using Agencourt AMPure magnetic beads (Beckman Coulter) according to the manufacturer's instructions, and analyzed by qPCR using SYBR Green technology (Applied Biosystems). The chromatin enrichment of each gene locus was calculated by standard curve method, normalized to 1% input. Relative enrichment values were normalized to a negative control region of the genome (IVL gene promoter). Primers are listed in Table S3.

ChIP library preparation.

DNA libraries for sequencing were prepared from approximately 10 ng DNA from ChIP samples using the KAPA Hyper (KR096100) library preparation kit according to the manufacturer's instructions (Kapa Biosystems).

ChIP data analysis

-Alignment

SEM and RS4;11 ChIP-seq fastq files were obtained from previously published datasets (GSE74812 and GSE38403, respectively).

Sequence reads in fastq format were mapped onto the reference human genome version hg38, Genome Reference Consortium GRCh38. The Illumina reads were aligned to the human genome using Bowtie2(Langmead and Salzberg, 2012). Reads that were uniquely aligned to chromosomal positions were retained and duplicate reads were removed from the aligned data using Picard tools (http://broadinstitute.github.io/picard/). Tag densities were generated from mapped bam files using the HOMER (http://homer.salk.edu/homer/index.html) "makeTagDirectory" command. Bedgraphs for displayed in the UCSC Genome Browser were generated using the HOMER "makeUCSCfile" command.

-Peak calling

FLAG-MLL-Af4

Regions of enrichment (peaks) of ChIP sequencing data were identified using DFilter software(Kumar et al., 2013) with recommended parameters (-bs=100 -ks=50 –refine).

SEM and RS4;11

Peaks were called using the HOMER findPeaks command (-style factor) and normalized to the respective input ChIP-seq tracks. Peaks of MLLN and AF4C were overlapped using bedtools (http://bedtools.readthedocs.org/en/latest/) “intersect” to generate MLL-AF4 peak sets.

Peak overlaps were defined by an exact intersection with no gaps tolerated. Gene annotations were performed using in-house scripts. Peaks were defined as binding to the promoter of a gene if located +/- 2kb within the transcription start site (TSS).

-Heat-maps

The MLL-Af4 and SEM MLL-AF4 peak files were sorted by MLL-Af4 (FLAG) or SEM MLL(N) ChIP-seq reads, respectively, under each peak. The sorted peak files were used with the HOMER “annotatePeaks” command alongside the tag directories of ChIP-seq tracks, to determine signal at these peaks. Heat-map matrices were visualized using Java TreeView (http://jtreeview.sourceforge.net/).

-Correlation matrix

ChIP-seq read coverage at SEM MLL-AF4 peaks was determined using deepTools (http://deeptools.readthedocs.io/en/latest/) “multiBamCoverage BED-file”. The output compressed numpy array (.npz) was plotted as a heat-map using deepTools “plotCorrelation” with the Pearson correlation method.

RT-PCR

RNA was reversed transcribed using MuLV Reverse Transcriptase and random hexamers (Applied Biosystems). The cDNA was then subject to qPCR using SYBR Green technology

(Roche). Expression level was calculated by ΔΔCt method, normalized to GAPDH. Primers are listed in Table S3.

RNA sequencing

1 ug total RNA was used for poly(A) RNA selection, followed by cDNA synthesis using PrepX mRNA Library kit (WaferGen) and Apollo 324 NGS automatic library prep system. Sample-specific index was added to the adaptor-ligated cDNA by PCR with index-specific primers for 13 cycles. The cluster generation of indexed libraries was carried out on cBot system (Illumina) using Illumina's TruSeq SR Cluster kit v3, and then sequenced on Illumina HiSeq system using TruSeq SBS kit to generate single-end 50 cycle reads. 20-50 million reads were generated for each sample.

Analysis of RNA sequencing data

-Alignment and identification of differentially expressed genes

Sequence reads were aligned to the human reference genome using the TopHat aligner, and reads aligning to each known transcript were counted using Bioconductor packages for next-generation sequencing data analysis(Huber et al., 2015). Transcript expression levels were estimated as reads per kilobase of transcript per million mapped reads (RPKM). For lymphoid leukemia study, RPKM data were imported into Qlucore Omics Explorer 3.1 software (Qlucore) for further analysis. To identify differentially expressed genes between MLL-Af4 and MLL-AF9 myeloid cells, the analysis was performed in edgeR Bioconductor package using generalized linear model likelihood ratio test for paired samples(Robinson et al., 2010), with a cutoff of FDR≤0.1 and fold change ≥1.5.

-Pathway enrichment analysis

To obtain MLL-AF4 patient gene signature, expression data from Stam et al. were downloaded from GEO database (GSE19475), expression data from Andersson et al. were obtained from Dr. Andersson (Andersson et al., 2015; Stam et al., 2010), and then imported into Qlucore. By comparing MA4 patients to non-MLL-fusion patients, significant differential genes were selected by built-in statistical functions ($P \leq 0.05$, $FDR \leq 0.1$, fold change ≥ 2) and defined as MA4 signature (Table S4). The expression of MA4 signature genes was evaluated in MLL-Af4 leukemic cells compared to control proB cells, the significant differentially expressed genes between two groups ($P \leq 0.05$) were ranked according to fold change as a heatmap and colored depending on whether they are upregulated (pink) or downregulated (green) in MA4 patients. GSEA analysis was performed as described(Subramanian et al., 2005). The same approach was used to evaluate B cell developmental stage specific genes association with MLL-Af4 and -AF9 leukemic cells. The proB and preB signatures were derived from Hystad et al (Table S5) (Hystad et al., 2007). For myeloid cell studies, the pathway enrichment analysis was performed separately for upregulated and downregulated genes using the LRpath methodology with the gene lists from the MSigDB database(Sartor et al., 2009).

-Cluster analysis

In order to test the similarity of MLL-Af4 gene expression to those of MA4 patients relative to patients with other MLL-fusions, the RPKM data of our MLL-Af4, -AF9 and control proB samples plus the Andersson dataset were imported into Qlucore. The batch effect of different datasets was corrected automatically by using "Eliminated Factor" function of the software. After correction, built-in principal component analysis and unsupervised hierarchical clustering

were performed based on the expression of a 100-gene discriminator derived by Andersson et al (Table S6), which best associates patient samples according to MLL-fusion partners. In addition, to test whether the gene signature derived from our model can be used to discriminate patient samples, the significant differentially expressed genes ($P \leq 0.05$, $FDR \leq 0.1$, fold change ≥ 1.5) between MLL-Af4 and MLL-AF9 CD45+ CD19+ leukemic cells were determined. To avoid batch effects that could skew the data, the comparison was performed using genes not having consistent significant variation between the two datasets irrespective of MLL fusions (~70% of total genes). A list of 430 genes was generated for cluster analysis (Table S7).

Supplemental References

Huber, W., Carey, V. J., Gentleman, R., Anders, S., Carlson, M., Carvalho, B. S., Bravo, H. C., Davis, S., Gatto, L., Girke, T.*, et al.* (2015). Orchestrating high-throughput genomic analysis with Bioconductor. Nat Methods *12*, 115-121.

Kumar, V., Muratani, M., Rayan, N. A., Kraus, P., Lufkin, T., Ng, H. H., and Prabhakar, S. (2013). Uniform, optimal signal processing of mapped deep-sequencing data. Nat Biotechnol *31*, 615-622.

Langmead, B., and Salzberg, S. L. (2012). Fast gapped-read alignment with Bowtie 2. Nat Methods *9*, 357-359.

Robinson, M. D., McCarthy, D. J., and Smyth, G. K. (2010). edgeR: a Bioconductor package for differential expression analysis of digital gene expression data. Bioinformatics *26*, 139-140.

Sartor, M. A., Leikauf, G. D., and Medvedovic, M. (2009). LRpath: A logistic regression approach for identifying enriched biological groups in gene expression data. Bioinformatics *25*, 211-217.

Subramanian, A., Tamayo, P., Mootha, V. K., Mukherjee, S., Ebert, B. L., Gillette, M. A., Paulovich, A., Pomeroy, S. L., Golub, T. R., Lander, E. S., and Mesirov, J. P. (2005). Gene set enrichment analysis: a knowledge-based approach for interpreting genome-wide expression profiles. Proc Natl Acad Sci U S A *102*, 15545-15550.